MICHIGAN STATE UNIVERSITY

CYCLOTRON LABORATORY

SPACE-TIME EVOLUTION OF NUCLEAR REACTIONS PROBED BY TWO-PROTON INTENSITY INTERFEROMETRY

W.G. GONG, W. BAUER, C.K. GELBKE, and S. PRATT

OCTOBER 1990

MSUCL-743

MSUCL-743
October 1990

"Space-time evolution of nuclear reactions probed by two-proton intensity interferometry"

W.G. Gong, W.Bauer, C.K. Gelbke
National Superconducting Cyclotron Laboratory
and Department of Physics and Astronomy,
Michigan State University, East Lansing, MI 48824, USA

and

S. Pratt
Department of Physics, University of Wisconsin, Madison, WI 53706, USA

Abstract

An approximate relation is derived which allows the calculation of the two-proton correlation function for any reaction model capable of predicting the classical single-particle phase-space distribution or Wigner function in the exit channel. The sensitivity of the calculated two-proton correlation functions to source radii and lifetimes is illustrated with simple parametrieations. More realistic calculations are presented for two different regimes of emission time scales: slow particle evaporation from equilibrated compound nuclei, as predicted from the Weisskopf formula, and fast nonequilibriua particle emission in intermediate energy nucleus-nucleus collisions, as predicted from the Boltsmann-Uehling-Uhlenbeck (BUU) transport equation.

PACS index: 25.70 Np

1. *Introduction*

Two particles, emitted at small relative momenta from an excited nuclear system, carry information about the space-time characteristics of the emitting source [1-24]. The shape of the two-proton correlation function reflects the interplay of the short-range nuclear interaction, the Pauli exclusion principle, and the long-range Coulomb interaction between the two emitted protons [1,2,14]. The attractive S-wave nuclear interaction leads to a pronounced maximum in the two-proton correlation function at relative momentum, $q \approx 20$ MeV/c, when the average distance upon emission is of the order of 10 fm or less [1]. The long-range Coulomb interaction and the Pauli exclusion principle give rise to a minimum at $q=0$. Some directional information can be provided by antisymmetrization effects [2,14,16] when $|\vec{q}\cdot\vec{r}|<h$, where $\vec{q}$ and $\vec{r}$ denote the relative momentum and position vectors upon emission.

In this article, we give a brief derivation of the general formalism which allows the calculation of two-proton correlation functions from the knowledge of the single-particle phase space density. The sensitivity of two-proton correlation functions to source radii and lifetimes is illustrated by means of simple analytical source parametrizations. Different regimes of emission time-scales are explored by giving specific examples for slow evaporative and fast non-evaporative particle emission processes, calculated with the Weisskopf evaporation formula and the Boltzmann-Uehling-Uhlenbeck transport equation, respectively.

The paper is structured as follows. In Section 2, we present a brief derivation of the general formalism which relates the two-proton correlation function to the single particle Wigner function. In Section 3, we illustrate the sensitivity of two-proton correlation functions to source radii and emission time scales by performing calculations for a number of simple source parametrizations. In Section 4, we give a brief review of the basic assumptions underlying the derivation of the BUU transport equation. Numerical results obtained by solving the BUU equation are presented in Section 5. Section 6 gives a brief review of the Weisskopf formula used for the calculation of particle evaporation from equilibrated compound nuclei; numerical

results are given in Section 7. A summary is given in Section 8. Detailed comparisons with recent experimental results will be given in a forthcoming paper [24].

2. *Correlation function formalism*

A number of formalisms have been published [1] which derive two-particle correlation functions from the knowledge of the emission function, $g(\vec{p},x)$, i.e. the probability of emitting a particle with momentum $\vec{p}$ from space-time point $x=(\vec{r},t)$. The derived expressions differ only in minor details and the predicted results are similar. Here, we derive an expression for the correlation function in most general terms assuming complete knowledge of all two-particle quantum mechanical matrix elements. We then introduce and justify approximations which allow practical calculations. For simplicity, we will restrict ourselves to the important case of correlations between two identical particles.

In the following, we will use four-vector notation to keep our formulae compact and manageable. However, our formalism is not relativistically covariant.

Our final expression for the two-particle correlation function is identical to the expressions given in refs. [2,14]:

$$R(\vec{P},\vec{q})+1 = C(\vec{P},\vec{q}) = \frac{\Pi(\vec{p}_1,\vec{p}_2)}{\Pi(\vec{p}_1)\Pi(\vec{p}_2)} =$$

$$= \frac{\int d^4x_1 d^4x_2 g(\vec{P}/2,x_1) g(\vec{P}/2,x_2) |\Phi(\vec{q},\vec{r}_1-\vec{r}_2-(t_2-t_1)\vec{P}/2m)|^2}{\int d^4x_1 g(\vec{P}/2,x_1) \int d^4x_2 g(\vec{P}/2,x_2)} . \qquad (1)$$

Here, $\Pi(\vec{p}_1,\vec{p}_2)$ and $\Pi(\vec{p})$ denote the two-particle and single-particle emission probabilities, $\vec{P}$ and $\vec{q}$ are the total and relative momenta, $\vec{P}=\vec{p}_1+\vec{p}_2$ and $\vec{q}=(\vec{p}_1-\vec{p}_2)/2$, respectively, and Φ is the relative wave function.

This expression was given in ref. [2] without derivation. It was derived in ref. [14] by using the sudden approximation for which the particles are assumed to be on shell in their final state and the mutual interaction is

switched on suddenly. Equation (1) was then derived assuming the thermal wavelength is much smaller than the size of the system. These approximations are not very well justified. Here, we start from the full quantum-mechanical expression for two-particle emission and show how, under most circumstances, we can justify a few approximations which lead to Eq. (1). Results obtained in many other formalisms are similar. For instance, in the literature on two-pion interferometry the function $g(\vec{P}/2,x)$ is often replaced by something similar, for example, $[g(\vec{p}_1,x)\cdot g(\vec{p}_2,x)]^{1/2}$. As long as the relative momentum $|\vec{q}|$ is much smaller than a characteristic momentum, $|\vec{p}|$, of $g(\vec{p},x)$ (such as $|\vec{p}|\approx\sqrt{3mT}$, where T is the temperature), there is little difference between the formalisms.

The complete matrix element for the creation of the n-body final state includes all information necessary for the calculation of correlation functions. Here we will derive an approximation in which the correlation function will only depend on properties of the one-body emission probability which can be extracted from the one-body matrix elements.

We start out by first considering the probability for creating two particles with final momenta $\vec{p}_1$ and $\vec{p}_2$ from sources 1 and 2 at space-time points x_1 and x_2:

$$\Pi(\vec{p}_1,\vec{p}_2) = |\int d^4x_1 d^4x_2 M_1(x_1)M_2(x_2)U(x_1,x_2:\vec{p}_1,\vec{p}_2)|^2 \ . \qquad (2)$$

Here, $U(x_1,x_2:\vec{p}_1,\vec{p}_2)$ is the evolution operator for particles created at x_1 and x_2 which end up in the asymptotic momentum states $\vec{p}_1$ and $\vec{p}_2$. The matrix element $M_i(x_i)$ creates the particle at x_i and the remaining collision products into a state which henceforth does not interact with the particle. In Eq. (2), we have assumed that the particles are emitted independently. This allows the factorization of the matrix element for two-body emission into the product of single-body elements.

By squaring the matrix elements and transforming to the new coordinates x_i (mean) and δx_i (relative), we obtain

$$\Pi(\vec{p}_1,\vec{p}_2) = \int d^4x_1 d^4\delta x_1 d^4x_2 d^4\delta x_2 S_1(x_1,\delta x_1)S_2(x_2,\delta x_2)W_{p_1,p_2}(x_1,\delta x_1,x_2,\delta x_2) \ . \qquad (3)$$

where

$$W_{\vec{p}_1,\vec{p}_2}(x_1,\delta x_1,x_2,\delta x_2) = U^{\dagger}(x_1+\delta x_1/2,x_2+\delta x_2/2:\vec{p}_1,\vec{p}_2) \\ U(x_1-\delta x_1/2,x_2-\delta x_2/2:\vec{p}_1,\vec{p}_2) \ , \tag{4}$$

and

$$S_1(x_1,\delta x_1) = M_1^{\dagger}(x_1+\delta x_1/2)M_1(x_1-\delta x_1/2) \ . \tag{5}$$

The expression becomes physically more transparent when the dependences on δx_i are replaced by dependences on the momenta, k_i, through four-dimensional Wigner transforms. As a result, we obtain:

$$\Pi(\vec{p}_1,\vec{p}_2) = \int d^4x_1 d^4x_2 d^4k_1 d^4k_2 \tilde{S}_1(x_1,k_1)\tilde{S}_2(x_2,k_2)\tilde{W}_{\vec{p}_1,\vec{p}_2}(x_1,k_1,x_2,k_2) \ , \tag{6}$$

with the Wigner transforms $\tilde{S}$ and $\tilde{W}$ defined by:

$$\tilde{S}_i(x,k) = \int d^4\delta x S_i(x,\delta x)e^{i\delta x\cdot k} \ , \tag{7}$$

and

$$\tilde{W}_{\vec{p}_1,\vec{p}_2}(x_1,k_1,x_2,k_2) = \int d^4\delta x_1 d^4\delta x_2 W_{\vec{p}_1,\vec{p}_2}(x_1,\delta x_1,x_2,\delta x_2)e^{-i\delta x_1\cdot k_1 - i\delta x_2\cdot k_2} \ . \tag{8}$$

For non-interacting distinguishable particles, the time evolution operators, U, in Eq. (2) become simple exponentials, and we obtain from Eq. (4) the relation $W_{\vec{p}_1,\vec{p}_2}=\exp(i\delta x_1\cdot p_1+i\delta x_2\cdot p_2)$. In this case, we can see from Eq. 8 that $\tilde{W}_{\vec{p}_1,\vec{p}_2}(x_1,k_1,x_2,k_2)=\delta^4(p_1-k_1)\delta^4(p_2-k_2)$, as expected: Non-interacting distinguishable particles retain their four-momentum after the emission.

The functions $\tilde{S}_i(x,k)$ are the quantum mechanical analogues of the emission probability for particles with four-momentum k from space-time point x. This can be seen from the following argument. Performing the same steps as above, but now for the single particle distributions, and making use of the relation $\tilde{W}_{\vec{p}}(x,k)=\delta^4(p-k)$, we obtain the result

$$\Pi(\vec{p}) = \int d^4x d^4k\ \tilde{S}(x,k)\delta^4(p-k)\ . \tag{9}$$

From here on, we will imply the on-shell condition $p^0 = E(\vec{p})$ when referring to the 0^{th} component of the asymptotic momentum. Equation (9) shows that the emission probability is given by:

$$g(\vec{p},x) = \tilde{S}(x,p)\ . \tag{10}$$

In order to obtain an expression for $\tilde{W}_{\vec{p}_1,\vec{p}_2}(x_1,k_1,x_2,k_2)$, we assume that the first emitted particle propagates freely for a time t_2-t_1 before it interacts with the second particle which is created at t_2. With this assumption, the evolution operator,

$$\tilde{U}(\vec{k}_1,t_1,\vec{k}_2,t_2:\vec{p}_1,\vec{p}_2) = (2\pi)^{-6} \int d^3x_1 d^3x_2 U(x_1,x_2:\vec{p}_1,\vec{p}_2) e^{-i\vec{k}_1\cdot\vec{x}_1 - i\vec{k}_2\cdot\vec{x}_2}\ , \tag{11}$$

for momentum states, $\vec{k}_i$, to evolve into the true scattering states, $\vec{p}_i$, can be written as

$$\tilde{U}(\vec{k}_1,t_1,\vec{k}_2,t_2:\vec{p}_1,\vec{p}_2) = \Phi(\vec{k}_1,\vec{k}_2:\vec{p}_1,\vec{p}_2)\cdot\exp\{iE_{12}t_2 + iE_1(t_1-t_2)\}\ . \tag{12}$$

Here E_{12} is the total kinetic energy of the proton pair, and Φ is the projection of the total wave function on the plane wave states $\vec{k}_1$ and $\vec{k}_2$.

If the emissions of the two particles are not far apart in time, the assumption of time-ordered emission entering Eq. (12) becomes questionable due to the uncertainty principle.

One can now calculate $\tilde{W}$ in terms of the wave function projection Φ:

$$\tilde{W}_{\vec{p}_1,\vec{p}_2}(x_1,k_1,x_2,k_2) =$$

$$\int d\delta t_1 d^3\delta\vec{k}_1 d\delta t_2 d^3\delta\vec{k}_2 \tilde{U}^{\dagger}(\vec{k}_1+\delta\vec{k}_1/2, t_1+\delta t_1/2, \vec{k}_2+\delta\vec{k}_2/2, t_2+\delta t_2/2:\vec{p}_1,\vec{p}_2)$$

$$\cdot\tilde{U}(\vec{k}_1-\delta\vec{k}_1/2, t_1-\delta t_1/2, \vec{k}_2-\delta\vec{k}_2/2, t_2-\delta t_2/2:\vec{p}_1,\vec{p}_2)$$

$$= \int d^3\delta k_1 d^3\delta k_2 d^3R_1 d^3R_2 \delta(k_1^0-E_1)\delta[k_2^0-(E_{12}-E_1)] f_2(\vec{k}_1,\vec{k}_2,\vec{R}_1,\vec{R}_2:\vec{p}_1,\vec{p}_2)$$

$$e^{-i\delta\vec{k}_1\cdot[\vec{x}_1+\vec{k}_1(t_2-t_1)/m-\vec{R}_1]-i\delta\vec{k}_2\cdot(\vec{x}_2-\vec{R}_2)} \quad . \tag{13}$$

Here, the symbol k_i^0 is the 0^{th} component of the four vector k_i. To arrive at the second part of Eq. (13), we performed Fourier transforms and made the linear approximation for the energy, $E(\vec{k}+\delta\vec{k})\approx E(\vec{k})+\delta\vec{k}\cdot\vec{k}/m$. The function f_2 introduced into Eq. (13) is the Wigner decomposition of the total two-particle density matrix:

$$f_2(\vec{k}_1,\vec{k}_2,\vec{R}_1,\vec{R}_2:\vec{p}_1,\vec{p}_2) = \int d^3\delta k_1 d^3\delta k_2 \exp(-i\delta\vec{k}_1\vec{R}_1-i\delta\vec{k}_2\vec{R}_2)$$

$$\Phi^*(\vec{k}_1+\delta\vec{k}_1/2,\vec{k}_2+\delta\vec{k}_2/2:\vec{p}_1,\vec{p}_2)\Phi(\vec{k}_1-\delta\vec{k}_1/2,\vec{k}_2-\delta\vec{k}_2/2:\vec{p}_1,\vec{p}_2)$$

$$= \int d^3\delta x_1 d^3\delta x_2 \exp(-i\delta\vec{x}_1\vec{k}_1-i\delta\vec{x}_2\vec{k}_2)$$

$$\Phi^*(\vec{R}_1+\delta\vec{x}_1/2,\vec{R}_2+\delta\vec{x}_2/2:\vec{p}_1,\vec{p}_2)\Phi(\vec{R}_1-\delta\vec{x}_1/2,\vec{R}_2-\delta\vec{x}_2/2:\vec{p}_1,\vec{p}_2) \quad . \tag{14}$$

We insert Eq. (13) into the expression for the two-particle probability, Eq. (6), perform the integration over k_i^0 and obtain

$$\Pi(\vec{p}_1,\vec{p}_2) = \int d^3\delta k_1 d^3\delta k_2 d^3R_1 d^3R_2 d^3k_1 d^3k_2 d^4x_1 d^4x_2 \tilde{S}(x_1,E_1,\vec{k}_1)\tilde{S}(x_2,E_{12}-E_1,\vec{k}_2)$$

$$f_2(\vec{k}_1,\vec{k}_2,\vec{R}_1,\vec{R}_2:\vec{p}_1,\vec{p}_2)e^{-i\delta\vec{k}_1\cdot[\vec{x}_1+\vec{k}_1(t_2-t_1)/m-\vec{R}_1]-i\delta\vec{k}_2\cdot(\vec{x}_2-\vec{R}_2)} \quad . \tag{15}$$

If we had used a different "reasonable" formula for Eq. (12) or kept more terms in the expansion of $E(\vec{k}+\delta\vec{k})$, we would have obtained the same formula as Eq. (15) except that the partition of energy into the source at x_1 and the source at x_2 would have been different. These details are not important since they will be absorbed into the approximation of the next paragraph.

In order to make the formalism tractable, that is depend only on $S(\vec{x},E,(\vec{k}_1+\vec{k}_2)/2)$, we now make the assumption that the product of the matrix elements $S_1 \cdot S_2$ depends weakly on the partition of the four-momentum. In order for the particles to interact, x_1 and x_2 must be very close together. The function $\tilde{S}$ should then have the same momentum dependence at both points. If

the momentum dependence is thermal, then the product of the Boltzmann distributions has no dependence on k_1-k_2. Even for arbitrary momentum dependence, the product $\tilde{S}_1 \cdot \tilde{S}_2$ has, to first order, no dependence on relative momentum. If we do not make the approximation of weak dependence on the partition of four-momentum, the formalism is intractable, unless we know quantum details of the emission matrix $\tilde{S}(k,x)$ for $k^0 \neq E(\vec{k})$. This assumption allows us to integrate over $d^3\delta k_i$ and d^3R_i and express the two-particle probability as:

$$\Pi(\vec{p}_1,\vec{p}_2) = \int d^3k_1 d^3k_2 d^4x_1 d^4x_2 \tilde{S}(x_1,E_{12}/2,(\vec{k}_1+\vec{k}_2)/2)\tilde{S}(x_2,E_{12}/2,(\vec{k}_1+\vec{k}_2)/2)$$

$$f_2(\vec{k}_1,\vec{k}_2,\vec{x}_1+\vec{k}_1(t_2-t_1)/m,\vec{x}_2:\vec{p}_1,\vec{p}_2) \ . \qquad (16)$$

Since the total momentum of the pair is conserved during the evolution towards their asymptotic momentum states, we can substitute $\vec{k}_1+\vec{k}_2=\vec{p}_1+\vec{p}_2:=\vec{P}$. We obtain

$$\Pi(\vec{p}_1,\vec{p}_2) = \int d^3k_1 d^3k_2 d^4x_1 d^4x_2 \tilde{S}(x_1,P/2)\tilde{S}(x_2,P/2)$$

$$f_2(\vec{k}_1,\vec{k}_2,\vec{x}_1+\vec{k}_1(t_2-t_1)/m,\vec{x}_2:\vec{p}_1,\vec{p}_2) \ . \qquad (17)$$

The emission function S is evaluated at the four-momentum $P=(E(\vec{P}),\vec{P})$. In general, the 0^{th} component of this four-vector is not equal to E_{12}. However, as long as $\vec{p}_1-\vec{p}_2$ is small, this difference can be neglected. This approximation allows us now to replace the function $\tilde{S}(x_i,P/2)$ with the single particle emission probability $g(\vec{P}/2,x)$, see Eq. (10). We can now calculate the two-particle probability in terms of single particle probabilities. It is prudent to make the same approximations in the expression for the single particle emission probabilities. Then the correlation function for non-interacting particles will remain at unity even when $\vec{p}_1-\vec{p}_2$ is not small.

Dividing the two-particle emission probability from Eq. (17) by the single particle emission probabilities thus yields for the two-particle correlation function:

$$C(\vec{P},\vec{q}) =$$

$$\frac{\int d^4x_1 d^4x_2 d^3k_1 d^3k_2 g(\vec{P}/2,x_1)g(\vec{P}/2,x_2)f_2(\vec{k}_1,\vec{k}_2,\vec{x}_1+\vec{k}_1(t_2-t_1)/m,\vec{x}_2:\vec{p}_1,\vec{p}_2)}{\int d^4x_1 d^3k_1 g(\vec{P}/2,x_1)f_1(\vec{k}_1,\vec{x}_1:\vec{p}_1)\int d^4x_2 d^3k_2 g(\vec{P}/2,\vec{x}_2)f_1(\vec{k}_2,\vec{x}_2:\vec{p}_2)} \quad . \tag{18}$$

Using the definition of the Wigner decompositions, Eq. (14), and the fact that the two-particle wave function can be factored into the center-of-mass wave function multiplied by the relative wave function,

$$\Phi(\vec{x}_1,\vec{x}_2:\vec{p}_1,\vec{p}_2) = \exp[-i(\vec{p}_1+\vec{p}_2)(\vec{x}_1+\vec{x}_2)/2]\phi[(\vec{p}_1-\vec{p}_2)/2,\vec{x}_1-\vec{x}_2] \quad , \tag{19}$$

one finds for the integrals over the Wigner functions f_1 and f_2:

$$\int d^3k_i f_1(\vec{k}_i,\vec{x}_i:\vec{p}) = 1 \quad , \tag{20}$$

$$\int d^3k_1 d^3k_2 f_2(\vec{k}_1,\vec{k}_2,\vec{x}_1,\vec{x}_2:\vec{p}_1,\vec{p}_2) = \int d^3(k_1+k_2) d^3(\frac{k_1-k_2}{2}) f_2(\vec{k}_1,\vec{k}_2,\vec{x}_1,\vec{x}_2:\vec{p}_1,\vec{p}_2)$$

$$= \int d^3(k_1+k_2) d^3(\frac{k_1-k_2}{2}) \delta^3(\vec{P}-\vec{k}_1-\vec{k}_2)$$

$$\int d^3\delta r \exp[i\delta\vec{r}\cdot(\vec{k}_1-\vec{k}_2)/2]\phi^*(\vec{q},\vec{x}_1-\vec{x}_2+\delta\vec{r}/2)\phi(\vec{q},\vec{x}_1-\vec{x}_2-\delta\vec{r}/2)$$

$$= |\phi(\vec{q},\vec{x}_2-\vec{x}_1)|^2 \quad . \tag{21}$$

Inserting these relations into Eq. (18) now yields our final result whioh was already given in Eq. (1).

The central assumption underlying our derivation is the approximation $\tilde{S}(x,E,\vec{k}_i) \approx \tilde{S}(x,E,(\vec{k}_1+\vec{k}_2)/2)$. This approximation becomes exact when the emission function $S(x,k)$ is broad, i.e. when its characteristic momentum is much larger than the relative momentum or the momentum spread of the resonance. In intermediate energy heavy-ion collisions this is an appropriate assumption since the characteristic momenta are of the order of magnitude of a few hundred MeV/c and the relative momenta of interest are smaller than 50 MeV/c. (The important momentum components for the ^{2}He "resonance" lie below 100 MeV/c.) If we keep the momentum dependence in Eq. (15), expanding $\vec{k}_i$ about $\vec{P}/2$, we can

show that this dependence cancels out in first order. Thus we expect the formalism to give very close to the correct answer, unless the characteristic momentum of the emission becomes quite small. Our derivation does not rely on the assumption that the system be semi-classical and that the thermal wavelength be much shorter than the size of bound states or even the size of the emitting system. Our result is valid as long as the product of $\tilde{S}_1 \cdot \tilde{S}_2$ depends only on $\vec{k}_1+\vec{k}_2$ and not $\vec{k}_1-\vec{k}_2$. For systems which sample many states, such as a thermal system, this is a good assumption. Since usually there is no knowledge of the matrix elements as a function of k^0, these approximations are the best we can do. Luckily, since we are interested in correlations for small relative momenta and since the characteristic momenta of the protons are sufficiently high, these are excellent approximations.

The correlation function $C(\vec{P},\vec{q})$ depends only on the final relative positions of all the particles with momentum $\vec{P}/2$. To make this more clear, we write Eq. (1) as:

$$C(\vec{P},\vec{q}) = \int d^3r F_{\vec{P}}(\vec{r}) |\phi(\vec{q},\vec{r})|^2 , \tag{22}$$

where $\vec{r} = \vec{r}_1-\vec{r}_2$ is the relative coordinate of the emitted particles. The function $F_{\vec{P}}(\vec{r})$ is defined by:

$$F_{\vec{P}}(\vec{r}) = \frac{\int d^3R f(\vec{P}/2,\vec{R}+\vec{r}/2,t_>) f(\vec{P}/2,\vec{R}-\vec{r}/2,t_>)}{|\int d^3r' f(\vec{P}/2,\vec{r}',t_>)|^2} . \tag{23}$$

where $\vec{R} = \frac{1}{2}(\vec{r}_1+\vec{r}_2)$ is the center-of-mass coordinate of the two particles. The Wigner function $f(\vec{p},\vec{r},t_>)$ is the phase-space distribution of particles of momentum $\vec{p}$ at position $\vec{r}$ at some time, $t_>$, after both particles have been emitted:

$$f(\vec{p},\vec{r},t_>) = \int_{-\infty}^{t_>} dt\, g[\vec{p},\vec{r}-\vec{p}(t_>-t)/m,t] . \tag{24}$$

For a given momentum $\vec{P}$, the correlation has three degrees of freedom, $\vec{q}$, which are a function of $F_{\vec{P}}(\vec{r})$. The most we can hope to extract from the correlation function is $F_{\vec{P}}(\vec{r})$, the normalized probability of two protons with the same

momentum $\vec{P}/2$ being separated by $\vec{r}$. We have shown in the derivation above that the calculation of $F_{\vec{P}}(\vec{r})$ requires only the knowledge of the final phase-space distributions or the emission probability $g(\vec{p},\vec{r},t)$.

3. *Discussion and illustrative calculations*

In this section, we will discuss the physical information contained in two-particle correlation functions, such as the source size and lifetime, and point out characteristic signatures of slowly cooling and explosive sources, respectively. The function $F_{\vec{P}}(\vec{r})$, Eq. (23), contains significant information about the dynamics of the collision. For instance, a long lived source will lead to an extended separation when $\vec{r}$ is parallel to the velocity $\vec{P}/2m$. Thus in addition to the spatial extent of $F_{\vec{P}}(\vec{r})$ one gains insight into the lifetime of the collision [14].

The $\vec{P}$ dependence yields insight into the dynamics of the collision. Both the spatial size and the lifetime can depend on the total momentum. Cooling [14,25,26] is signified by increasingly large lifetimes for particles with smaller energies. We discuss this later in the section on the compound nucleus. Collective explosive flow is signaled by short lifetimes and shrinking apparent source dimensions for increasing energy [27]. There should be a transition in reaction mechanisms, from evaporative to exploding, at excitation energies near the nuclear binding energy. This is the dynamical equivalent of the liquid-gas phase transition. At low excitation, the nuclear matter slowly evaporates particles, cooling like a hot liquid drop. At sufficiently high excitation, nuclear matter explodes and expands to fill the available volume, like a gas. This is also discussed in ref. [14].

The relative wave function, $\phi(\vec{q},\vec{r})$, is influenced by three different effects: identical particle interference, short range hadronic interaction, and the Coulomb repulsion of the protons. We briefly discuss how these three effects contribute to the correlation function and how the resulting correlations can be used to determine $F_{\vec{P}}(\vec{r})$.

To calculate the relative wave function numerically, we solved the Schrödinger equation for the ℓ=0 and ℓ=1 partial waves. For the total wave function, $\phi(\vec{q},\vec{r})$, we used the full solution Coulomb waves [28], $\phi_c(\vec{q},\vec{r})$, and

added the modification $\delta\phi(\vec{q},\vec{r})$ which is the contribution to the relative wave function from the first two partial waves minus the contribution which would have occurred if the strong interaction were absent. The Schrödinger equation was solved with the Reid soft core potential [29].

For identical non-interacting particles, the squared wave function has the form: $|\phi(\vec{p},\vec{r})|^2 \propto [1\pm\cos(2\vec{p}\cdot\vec{r})]$. In that case, the invèrse Fourier transform of the correlation function would yield the complete three-dimensional function $F_{\vec{p}}(\vec{r})$. For spin-half particles, the correlation function is reduced to one half at $|\vec{q}|=0$ and returns to unity with a width of $q_x \approx 1/R_x$. Experiments that gate on the direction of the relative momentum can then determine all three spatial dimensions of $F_{\vec{p}}(\vec{r})$.

Coulomb interactions yield a dip in the correlation function which goes to zero as $\vec{q}$ approaches zero. As long as the characteristic dimensions of $F_{\vec{p}}(\vec{r})$ are much smaller than the two-proton Bohr radius of 58 fm, the shape of the dip does not depend on the shape or size of the source but only on the Gamov factor. For larger sources, the Coulomb interaction, too, provides information about both the source size and, to a weak degree, on the shape. The Coulomb dip in the correlation function at $|\vec{q}|=0$ will diminish for large sources. The most unfortunate aspect of the Coulomb interaction is that the Coulomb dip lessens the number of available pairs at small relative momentum, making it more difficult to see the effects of identical particle interference.

Strong interactions provide excellent gauges of the size of smaller sources, $R \lesssim 10$ fm. The ^{2}He "resonance" appears as a bump in the proton-proton correlation function at a relative momentum of 20 MeV/c. (Strictly speaking, the ^{2}He "resonance" is not a resonance, since the phase shift does not increase by 90°, but only by about 60°.) The size of the bump is proportional to the percentage of pairs whose relative position is within the size of the nearly bound state. Thus the height goes roughly as R^{-3}. This provides a very sensitive test of the size, but not of the shape.

For typical source sizes of about 5 fm, all three effects are important. Choosing a distribution $F_{\vec{p}}(\vec{r})$ that fits the correlation function requires more than just the appropriate size as measured by a single parameter. One must

have $F_{\vec{p}}(\vec{r})$ correct for large $\vec{r}$ in order to fit the correlation function at low $\vec{k}$ in the Coulomb dip and one must have $F_{\vec{p}}(\vec{r})$ correct at small $\vec{r}$ in order to fit the height of the correlation function. If the source is not so large that the Coulomb dip erases the effect of identical particle interference, the shape must be chosen correctly as well to fit the correlation function for different directions of $\vec{q}$. Thus all the physical characteristics of $F_{\vec{p}}(\vec{r})$ can be thoroughly tested with correlation measurements. In the following subsections we illustrate some these qualitative expectations by calculations performed for simple analytical emission sources.

3.1. *Spherical sources of negligible lifetime*

The relative importance of antisymmetrization and the nuclear and Coulomb interactions depends on the size of the emitting system. In order to provide a quantitative comparison of these effects, we have calculated two-proton correlation functions for Gaussian sources of negligible lifetime,

$$g(\vec{p},\vec{r},t) = \rho(r)\delta(t-t_0) = \rho_0 \exp(-r^2/r_0^2)\delta(t-t_0) \ , \qquad (25)$$

in which the nuclear interaction and the Pauli principle were turned off successively. These calculations are compared in Fig. 1 for a number of representative radius parameters (r_0 = 2.5, 5, 10, 20 fm) . The solid curves show the results of the full calculations which include the nuclear and Coulomb interactions and the Pauli exclusion principle. The dotted lines show calculations for which the nuclear interaction has been turned off; these calculations still include quantum effects of the two-proton Coulomb interaction and the antisymmetrization of the relative wave function. The dashed curves represent calculations for which both the nuclear interaction and the antisymmetrization of the relative wave function have been turned off. (These latter calculations differ from classical Coulomb trajectory calculations [17] since the Coulomb repulsion between the two protons is treated quantum mechanically. For large source dimensions or emission from long-lived sources, this difference should be of minor importance.) For radius parameters, $r_0 \lesssim 10$ fm, both the antisymmetrization of the relative wave function and the nuclear interaction have important effects on the detailed shape of the calculated correlation functions. For much larger source dimensions, $r_0 \gtrsim 20$ fm, the

Coulomb interaction dominates and the neglect of the Pauli principle and the nuclear interaction can be justified [17].

Most analyses of fast-particle-emission processes [3-5,10-13,15-18] have used sources of negligible lifetime with spherically symmetric Gaussian density distributions, Eq. (25). For spherically symmetric sources, the shape of the two-proton correlation function is rather insensitive to details of the density profile. To illustrate this point, we compare the shapes of two-proton correlation functions calculated for sources of negligible lifetime with Gaussian, Eq. (25), and uniform sharp-sphere density distributions,

$$g(\vec{p},\vec{r},t) = \rho_s(r)\delta(t-t_0) = \rho_0\Theta(r)\Theta(R_s-r)\delta(t-t_0) \ . \qquad (26)$$

In Eq. (26), R_s is the sharp sphere radius and $\Theta(x)$ is the unit step function which vanishes for negative arguments. The solid and dotted curves in Fig. 2 represent calculations performed with Eqs. (25) and (26), respectively. In these calculations, the radius parameters have been adjusted to match the magnitudes of the maxima at q≈20 MeV. The correlation functions calculated for these rather different density profiles are virtually identical in shape. Previously, Gaussian source parameters, r_0, have been translated [1] into equivalent sharp sphere radii, R_s, by employing the approximate relation, $R_s \approx (5/2)^{1/2} r_0$. This relation can be justified by equating the rms radii of the two density distributions. Equivalent radii, r_0 and R_s, of the two density profiles can also be defined by the requirement that the calculated correlation functions have maxima of identical height. Such equivalent radii are indicated by X-shaped symbols in Fig. 3. These equivalent radii can be rather well described by the relation $R_s = 1.493 r_0 + 0.0475$ fm; this relation is represented by the solid curve in Fig. 3. For comparison, the analytically derived relation, $R_s = (5/2)^{1/2} r_0$, is indicated by the dotted curve; it is a surprisingly good approximation.

3.2. *Spherical sources of finite lifetime*

In order to illustrate the sensitivity of the shapes of two-proton correlation functions to the decay time of the emitting system, we have performed calculations under the simplifying assumption that particles are emitted from a spherical volume of radius R_s according to a simple exponential law,

$$g(\vec{p},\vec{r},t) \propto \rho_0\theta(r)\theta(R_S-r)\theta(t)ke^{-k^2/2mT-t/\tau} , \qquad (27)$$

where T and τ denote the (constant) source temperature and lifetime, respectively.

Calculations for two-proton correlation functions, integrated over all relative orientations between $\vec{P}$ and $\vec{q}$, are shown in Fig. 4. The parameters used in these calculations are given in the figure. The upper panel of the figure illustrates the sensitivity to the lifetime of the emitting system for proton pairs of total momentum, $P_{c.m.}$ = 300 MeV/c, measured in the rest frame of the emitting source. The calculated two-proton correlation functions exhibit considerable sensitivity to lifetimes of the order of 30-3000 fm/c. For much shorter lifetimes, the shape of the correlation function becomes dominated by the spatial dimension of the emitting system; for much longer lifetimes the correlations disappear. The lower panel of Fig. 4 illustrates how the correlation function depends on the total momentum of the emitted proton pairs for the case of a fixed lifetime, τ=100 fm/c. The calculated correlations become more pronounced for smaller total momenta, i.e. for particles emitted with lower kinetic energies. This dependence can be understood in terms of the spatial extent of the Wigner distribution. The longitudinal dimension of the apparent source is of the order of $(P_{c.m.}/2m_p)\tau$, where m_p denotes the proton mass. For fixed lifetime, τ, this quantity increases for larger values of $P_{c.m.}$ and the correlation function becomes attenuated. Such a momentum dependence stands in contrast to experimental observations [4,10-13,16,23,24] and is opposite to that calculated for emission from compound nuclei for which the effects of cooling produce a strong momentum dependence of the effective decay times, see also the discussion in Section 7.

Figure 5 illustrates the dependence of the two-particle correlation function on the angle, $\Psi = \cos^{-1}\{\vec{P}\cdot\vec{q}/Pq\}$, between the relative and total momentum vectors of the two-proton pair. As was done in the experimental analysis of ref. [24], we define transverse and longitudinal correlation functions by the cuts $|\cos\Psi| \geq 0.77$ (Ψ=0°-40° or 140°-180°) and $|\cos\Psi| \leq 0.5$ (Ψ=60°-120°). Different panels of Fig. 5 show transverse and longitudinal correlation functions calculated for different lifetimes τ=0, 10, 30, 100, 300, 1000 fm/c. In these calculations, the total momentum of the proton pair was kept constant at

$P_{c.m.}$=300 MeV/c. For very short lifetimes, $\tau \lesssim 10$ fm/c, the apparent source is essentially spherical in shape and life-time effects are negligible for the calculation of the two-proton correlation function. For an intermediate time-window, $\tau \approx 30$-300 fm/c, longitudinal and transverse correlation functions are sensitive to the lifetime of the emitting system. For larger lifetimes, $\tau \gtrsim 1000$ fm/c, this sensitivity is essentially lost as the average separation between emitted particles becomes so large that antisymmetrization effects become negligible. In fact, for extremely large lifetimes the effect is reversed because Coulomb induced correlations contain a weak amount of directional information. The Coulomb force is parallel to the relative displacement of the protons; therefore, the Coulomb hole in the correlation function will be strongest when the relative momentum is parallel to the longest dimension of the pair's separation. For long-lived sources this is the longitudinal direction. Comparisons of longitudinal and transverse correlation functions yield the strongest information about the lifetime of the emitting system for lifetimes of the order of 30-300 fm/c. By more judicious choices of the gates on $P_{c.m.}$, one may stretch the sensitivity of such measurements beyond these rough boundaries.

4. *BUU transport equation for collision dynamics*

In this section, we briefly review the derivation of the BUU transport equation which provides the basis for microscopic calculations for nonequilibrium particle emission in intermediate energy nucleus-nucleus collisions. We start with the Schrödinger equation of the N-particle system,

$$i\,\partial_t \Psi = H\Psi \ . \tag{28}$$

Here, H is the N-particle Hamiltonian and Ψ is the N-particle wave-function. From Ψ, one constructs the N-particle density,

$$\rho^{(N)} = \Psi\Psi^* \ , \tag{29}$$

which leads to the von-Neumann equation of motion:

$$i\partial_t \rho^{(N)} = [H,\rho^{(N)}] \ . \tag{30}$$

We introduce the reduced density matrices via

$$\rho^{(n)}(\vec{r}_1,\ldots,\vec{r}_n;\vec{r}_1',\ldots,\vec{r}_n') =$$

$$\frac{1}{(N-n)!}\int d^3r_{n+1}\cdots d^3r_N d^3r'_{n+1}\cdots d^3r'_N \rho^{(N)}(\vec{r}_1,\ldots,\vec{r}_N;\vec{r}_1',\ldots,\vec{r}_N') \ . \qquad (31)$$

Inserting Eq. (31) into Eq. (30), leads to the BBGKY hierarchy of the reduced density matrices. This hierarchy links the time derivative of $\rho^{(n)}$ to $\rho^{(n+1)}$. The lowest two member's of the BBGKY hierarchy are:

$$i\partial_t\rho^{(1)}(\vec{r}_1,\vec{r}_1') = -\frac{1}{2m}(\nabla^2_{r_1}-\nabla^2_{r_1'})\rho^{(1)}(\vec{r}_1;\vec{r}_1')$$

$$+\int d^3r_2[v(\vec{r}_1,\vec{r}_2)-v(\vec{r}_1',\vec{r}_2)]\rho^{(2)}(\vec{r}_1,\vec{r}_2;\vec{r}_1',\vec{r}_2) \qquad (32)$$

and

$$i\partial_t\rho^{(2)}(\vec{r}_1,\vec{r}_2;\vec{r}_1',\vec{r}_2') = -\frac{1}{2m}\sum_{i=1}^{2}(\nabla^2_{r_i}-\nabla^2_{r_i'})\rho^{(2)}(\vec{r}_1,\vec{r}_2;\vec{r}_1',\vec{r}_2')$$

$$+[v(\vec{r}_1,\vec{r}_2)-v(\vec{r}_1',\vec{r}_2')]\rho^{(2)}(\vec{r}_1,\vec{r}_2;\vec{r}_1',\vec{r}_2')$$

$$+\sum_{i=1}^{2}\int d^3r_3[v(\vec{r}_i,\vec{r}_3)-v(\vec{r}_i',\vec{r}_3)]\rho^{(3)}(\vec{r}_1,\vec{r}_2,\vec{r}_3;\vec{r}_1',\vec{r}_2',\vec{r}_3) \ . \qquad (33)$$

A closed solution of the equations of this hierarchy is only possible, if one truncates at a level n and with it neglects (n+1)-body correlations. Truncating at n=1, neglecting two-body correlations, and approximating $\rho^{(2)}$ as an antisymmetrized product of one-body densities, one obtains the TDHF equations:

$$i\partial_t\rho^{(1)} = [h,\rho^{(1)}] \ , \qquad (34)$$

where h is the single particle Hamiltonian,

$$h(\vec{r},\vec{r}') = -\delta^3(\vec{r}-\vec{r}')\frac{1}{2m}\nabla^2_r + \delta^3(\vec{r}-\vec{r}')\int d^3r_2\rho^{(1)}(\vec{r};\vec{r}_2)v(\vec{r},\vec{r}_2)$$

$$-\rho^{(1)}(\vec{r},\vec{r}')v(\vec{r},\vec{r}') \ . \qquad (35)$$

Performing a Wigner-transformation gives the Vlasov equation:

$$\partial_t f(\vec{p},\vec{r},t) + \frac{\vec{p}}{m}\cdot\vec{\nabla}_r f(\vec{p},\vec{r},t) - \vec{\nabla}_r U(\vec{r})\cdot\vec{\nabla}_p f(\vec{p},\vec{r},t) = 0 \ . \tag{36}$$

In Eq. (36), $U(\vec{r})$ is the mean field or Hartree potential,

$$U(\vec{r}) = \int d^3r_2 v(\vec{r},\vec{r}_2)\rho(\vec{r},\vec{r}_2) \ , \tag{37}$$

and $f(\vec{p},\vec{r},t)$ is the Wigner-transform of the single-particle density matrix,

$$f(\vec{p},\vec{r},t) = \int d^3s \ \rho^{(1)}(r-\frac{s}{2},r+\frac{s}{2})e^{i\vec{p}\vec{s}} \ . \tag{38}$$

In the derivation of Eq. (36), the semiclassical approximation has been used. This approximation is valid since typical wavelengths ($\lambda\approx 2.5$ fm for p=500 MeV/c) are shorter than the size of the regions with the mean field (typically of the order of 8 fm diameter). The TDHF and Vlasov approximations to the many-body problem are pure one-body theories in mean field approximation in which all multi-particle correlations are neglected.

A truncation of the BBGKY hierarchy which includes two-body correlations, but neglects three- and higher-particle correlations leads to the Boltzmann-Uehling-Uhlenbeck (BUU) equation:

$$\begin{aligned}\partial_t f(\vec{p},\vec{r},t) + \frac{\vec{p}}{m}\cdot\vec{\nabla}_r f(\vec{p},\vec{r},t) - \vec{\nabla}_r U(\vec{r})\cdot\vec{\nabla}_p f(\vec{p},\vec{r},t) = \\ \frac{1}{2\pi^3 m^2}\int d^3q_1' d^3q_2 d^3q_2' \delta\{\frac{1}{2m}(p^2+q_2^2-q_1'^2-q_2'^2)\}\delta^3(\vec{p}+\vec{q}_2-\vec{q}_1'-\vec{q}_2')\frac{d\sigma}{d\Omega} \\ \times\{\hat{f}(\vec{q}_1',\vec{r},t)\hat{f}(\vec{q}_2',\vec{r},t)[1-\hat{f}(\vec{p},\vec{r},t)][1-\hat{f}(\vec{q}_2,\vec{r},t)] \\ - \hat{f}(\vec{p},\vec{r},t)\hat{f}(\vec{q}_2,\vec{r},t)[1-\hat{f}(\vec{q}_1',\vec{r},t)][1-\hat{f}(\vec{q}_2',\vec{r},t)]\} \ .\end{aligned} \tag{39}$$

In Eq. (39), $\hat{f}(\vec{p},\vec{r},t)$ is the phase-space-density averaged over one phase space cell. The left-hand side of the equation is the Vlasov term describing the temporal change of the one-body Wigner-function, $f(\vec{p},\vec{r},t)$, due to the interaction of the nucleons with the mean field. The right-hand side is the collision

integral which represents the effects of the correlations due to two-body collisions on the one-body Wigner-function. Equation (39) was first obtained by Nordheim [30] as a quantum mechanical extension of the Boltzmann equation which incorporates Fermion statistics.

Equation (39) is solved by using the pseudo-particle method [31]. In this method one compares the left-hand side of the equation to the complete differential of f:

$$\frac{d}{dt} f(\vec{p},\vec{r},t) = \frac{\partial}{\partial t} f(\vec{p},\vec{r},t) + \frac{d\vec{r}}{dt}\cdot\vec{\nabla}_r f(\vec{p},\vec{r},t) + \frac{d\vec{p}}{dt}\cdot\vec{\nabla}_p f(\vec{p},\vec{r},t) \ . \qquad (40)$$

From Eqs. (39) and (40), one obtains a set of six coupled first-order equations for every occupied phase-space point:

$$\frac{dr_i}{dt} = \frac{p_i}{m} \ , \qquad (41)$$

$$\frac{dp_i}{dt} = I_i(\vec{p}) - \frac{\partial}{\partial r_i} U(\vec{r}) \ . \qquad (42)$$

Here, $I_i(\vec{p})$ is the change in momentum p_i due to nucleon-nucleon collisions (i=1,2,3). The differential equations can be interpreted as the classical Hamiltonian equations of motion for a pseudo-particle. Since the total occupied phase space is proportional to the number of nucleons, it is convenient to specify the total number of phase space points per nucleon as a measure for the numerical precision with which Eq. (39) is solved. In the present calculations, we have used up to 700 pseudo-particles per nucleon, resulting in a total of up to 172,200 coupled first order differential equations which were solved simultaneously. The average phase space occupancies used to determine the effects of the Pauli principle in the collision integral were determined from the coordinates and momenta of the pseudo-particles. The cell size for averaging was chosen to be $\frac{1}{4}(h/2\pi)^3$.

5. *Two-proton correlation functions predicted by BUU equation*

Since BUU is basically a theory describing the time evolution of the one-body phase-space distribution function, it seems at first sight surprising that it could be used to calculate two-particle correlation functions.

Previously, it was shown [32-36] that the main features of two-proton coincidences at large angles are explained by the effects due to total momentum conservation, finite particle number, and/or collective motion in the reaction plane without requiring information about the detailed two-particle correlation function. However, within the formalism outlined in Section 2, the knowledge of the one-body phase-space distribution function is sufficient for the calculation of the two-proton correlation function at small relative momenta and the characterization of the size and lifetime of the reaction zone formed in the nuclear collision.

We solve the BUU equation by numerical methods which are similar to the ones introduced by ref. [37], see also ref. [38]. The major new numerical technique used in our present calculations is the treatment of the Pauli exclusion principle. By explicitly storing $\hat{f}(\vec{p},\vec{r},t)$ on a six-dimensional lattice in every time-step, we were able to greatly speed up the computer program without relaxing the accuracy of the treatment of the Pauli-exclusion principle [39]. In our calculations of the correlation functions, appropriate averages over impact parameter, orientation of the reaction plane, and the indicated gates on the total momentum and the angle, Ψ, between the relative and total momentum of the two protons were taken into account.

In our "standard" calculations, the Wigner functions of emitted particles were constructed from nucleons emitted during a time interval of Δt_e=140 fm/c following initial contact of the colliding nuclei. Nucleons were considered as emitted when, during this time interval, the surrounding density fell below $\rho_e=\rho_0/8$ and when subsequent interaction with the mean field did not cause recapture into regions of higher density. This test for recapture was continued over a time interval of Δt=180 fm/c after contact. The finite size of our lattice did not allow us to explore much larger emission times. However, the consideration of much larger emission times would not necessarily lead to more reliable results since, in our present approximation, the nuclei are not stable over long time scales and the BUU calculations become inaccurate due to spurious decays.

While our particular choice of the parameters Δt_e and ρ_e is reasonable, it involves a certain degree of arbitrariness. The sensitivity of the calculations to different choices of the emission time interval, Δt_e, and the freeze-out density, ρ_e, is illustrated in Fig. 6. Larger emission time intervals reduce the height of the maximum of the correlation function at q≈20 MeV/c due to an increase of the average emission time. On the other hand, smaller freeze-out densities lead to a slight increase in the height of the maximum of the correlation function. This can be understood as follows: lower emission densities select subsets of particles considered as emitted for higher freeze-out densities by eliminating late emissions (i.e. particles which have not yet reached the lower densities) and thus selecting particles which had left the higher density regime at earlier times. The corresponding reduction of the average temporal separation between emitted particles leads to enhanced correlations. Typically, different reasonable choices of Δt_e and ρ_e introduce uncertainties of the order of 5-10% into the magnitude of the predicted correlation functions. However, in some instances these uncertainties can be larger.

The two major ingredients entering into Eq. (39) are the mean field potential, $U(\vec{r})$, and the nucleon-nucleon cross section, $d\sigma/d\Omega$. In principle, one should be able to derive both from a fundamental nucleon-nucleon interaction, as has been done in some G-matrix calculations. In this paper, however, we proceed differently and use the conventional density-dependent Skyrme-type parametrization,

$$U(\rho) = A(\rho/\rho_0) + B(\rho/\rho_0)^{\sigma}, \tag{43}$$

where the parameters A and B are determined by the nuclear matter binding energy and the saturation density of nuclear matter at $\rho=\rho_0$. A choice of $\sigma=2$ results in A=-124 MeV and B=70.5 MeV and a nuclear compressibility of K = 380 MeV. This set of parameters is referred to as the "stiff" equation of state. The "soft" equation of state, with K=200 MeV, corresponds to the parameter set, $\sigma=7/6$, A=-356 MeV, and B=303 MeV. The simple parametrization, Eq. (43), is only chosen to investigate the possible sensitivity of our calculations to the value of the nuclear compressibility.

We approximate the in-medium nucleon-nucleon cross section, $d\sigma/d\Omega$, by the energy-dependent free nucleon-nucleon cross section, $d\sigma_{NN}/d\Omega$, parametrized from experimental data. Since the exact value of the in-medium nucleon-nucleon cross section has attracted some recent attention, we also vary this input by multiplying the experimental $d\sigma_{NN}/d\Omega$ by different factors ranging from 0 to 1.

For our numerical example, we calculate two-proton correlation functions for protons emitted at the laboratory angles $\theta_{lab} \approx 25^\circ \pm 9^\circ$ for $^{14}N+^{27}Al$ collisions at E/A=75 MeV, in close correspondence to the measurements of ref. [24]. Unless stated differently, we will use the stiff equation of state and in-medium cross sections equal to the experimental free nucleon-nucleon cross sections.

Figure 7 shows correlation functions calculated from Wigner functions predicted by the BUU equation using various assumptions on the in-medium nucleon-nucleon cross section and the stiffness of the equation of state. Individual panels of the figure show correlation functions calculated for different values of the total laboratory momenta, P, of the proton pairs. The solid and dotted curves show correlation functions predicted for the stiff and soft equations of state, using $d\sigma/d\Omega = d\sigma_{NN}/d\Omega$. These two calculations are very similar, indicating little sensitivity of the two-proton correlation functions to the stiffness of the equation of state. The solid, dashed, dot-dashed, and dot-dot-dashed curves represent calculations with the stiff equation of state performed with the assumption that the in-medium nucleon-nucleon cross-section is equal to 1.0, 0.8, 0.5, and 0.0 times the free nucleon-nucleon cross section. For $P \lesssim 700$ MeV/c, the predicted correlation functions become more pronounced for decreasing values of $d\sigma/d\Omega$ indicating that the space-time characteristics of the emitting system is more sensitive to the magnitude of the in-medium nucleon-nucleon cross section than to the stiffness of the equation of state.

Figure 8 compares the detailed shapes of two-proton correlation functions predicted for different space-time geometries. The solid points show correlation functions predicted from the BUU equation, averaged over the indicated

range of total momenta, P, of the proton pairs. These calculations are in excellent agreement with existing data [24]. The solid curve shows results obtained for instantaneous emission from a Gaussian source, Eq. (25), with radius parameter r_0=4.5 fm. The two-proton correlation function calculated for the Gaussian source, exhibits a narrower maximum than that calculated for the more realistic density distribution obtained by means of the BUU equation. This difference in shape can be attributed to the fact that sources predicted by the BUU equation are non-spherical. To illustrate the sensitivity of the shape of two-proton correlation functions to the source geometry, we show the correlation function predicted for emission from a source consisting of two sharp spheres of negligible lifetime. Both spheres were assumed to have radii of R_g=5 fm, and the centers of the two spheres were assumed to be separated by a distance of d=20 fm and aligned along the beam direction. The correlation function for this two-source distribution is depicted by the dashed curve in Fig. 8, it has a wider maximum than the single Gaussian source distribution and is rather similar in shape to that predicted from the BUU calculations. (Remember: two-proton correlation functions obtained for single spherical sources of sharp sphere and Gaussian density profiles are virtually indistinguishable in shape; see also the discussion of Figs. 2 and 3.)

Figures 9 and 10 depict the space-time evolution of the collision process as predicted by the BUU equation. Figure 9 shows the time evolution of the nucleon density in the reaction plane for a $^{14}N+^{27}Al$ collision at E/A=75 MeV and an impact parameter of 2 fm. Different panels of the figure represent snapshots taken at the indicated times after contact of the colliding nuclei. The calculations predict that the two colliding nuclei essentially survive the collision and separate into two hot nuclear objects which may then decay on longer time scales for which BUU calculations cannot make accurate predictions. More relevant for the calculations of two-proton correlation functions is the density distribution of the emitted nucleons in the reaction plane, shown in Fig. 10 for selected times after the initial contact of the colliding partners. The distribution of emitted nucleons clearly undergoes an evolution from a near-spherical source at early times to a two-source distribution at larger times. This two-source distribution at larger times may explain the similarity of the correlation functions obtained for a two-sphere distribution with that predicted by the BUU calculations.

The non-spherical shapes of the Wigner functions predicted by the BUU calculations should be reflected in differences between longitudinal and transverse correlation functions. Longitudinal and transverse correlation functions predicted by BUU calculations are shown in Fig. 11. We have adopted the angular cuts, $\Psi=\cos^{-1}(|\vec{P}\cdot\vec{q}|/|\vec{P}||\vec{q}|)=0^\circ-40^\circ$ and $60^\circ-90^\circ$, for the calculation of longitudinal and transverse correlation functions, respectively. For the transverse correlation functions, we define the in-plane and out-of-plane directions by constraints on the azimuthal angle, Φ, of the relative momentum vector, $\vec{q}$, in a coordinate system with z-axis parallel to the total momentum vector, $\vec{P}$, of the proton pair. Defining $\Phi=0^\circ$ as the plane spanned by the beam direction and $\vec{P}$, the in-plane transverse correlation function corresponds to the cut $|\Phi-n\pi|\leq 30^\circ$ (n=0,1,2); the out-of-plane transverse correlation function corresponds to the cut $|\Phi-(2n+1)\pi/2|\leq 30^\circ$ (n=0,1). Different panels of the figure show the results for the indicated cuts on the total momenta of the proton pairs. In general, the out-of-plane transverse correlation functions are smaller than the in-plane transverse correlation functions since they are less affected by finite lifetime effects and collective velocity components. At low momenta, the longitudinal correlation function is more pronounced than the transverse correlation functions, possibly due to slow emission times; at higher momenta, longitudinal and in-plane transverse correlation functions are comparable in magnitude.

Details of the Wigner function must depend on the impact parameter of the collision. The predicted dependence is illustrated in Fig. 12; the various cuts on the total momentum of the proton pairs are indicated for the individual panels of the figure. In order to summarize the predicted trends, Fig. 13 shows the heights of the maxima of the calculated correlation functions as a function of P for different ranges of impact parameters.

For small impact parameters, b=0.5-2.5 fm, the predicted correlation functions increase in magnitude as a function of increasing total momentum of the emitted particles, consistent with shorter time scales for the emission of more energetic particles.

For peripheral collisions, b=5-7 fm, the calculated correlations are weakest for proton pairs with very high, P≈800 MeV/c, or very low momenta,

$P \lesssim 300$ MeV/c; they are largest at intermediate momenta, $P \approx 500$ MeV. This correlation pattern may be understood in terms of emission from fairly well defined projectile and target-like sources. Proton pairs of low and high momenta correspond to low-energy emissions in the rest frames of target and projectile-like sources, respectively. More energetic emissions from these sources are selected by intermediate momenta. For these emissions the correlation functions are expected to be enhanced because of the reduced size of the participant zone and/or because of shorter emission time scales. However, nucleon-nucleon collisions appear to play only a minor role since the the maximum of the correlation function at $P \approx 500$ MeV/c remains when the in-medium nucleon-nucleon cross section is set to zero.

For intermediate impact parameters, $b \approx 3$-4.5 fm, the predicted momentum dependence is weak, most likely because of overlapping contributions from participant and spectator regions.

For total momenta, $P \lesssim 700$ MeV/c, more pronounced correlations are observed for peripheral than for central collisions - in accordance with a simple geometric interpretation of the size of the reaction zone. However, for protons emitted with velocities higher than the beam velocity, $P > 2p_{beam} \approx 760$ MeV/c, the maxima of the predicted correlation functions are larger for central than for peripheral collisions. Apparently, high energy particles from central collisions are emitted on a very fast time scale. It may be speculated that such fast emission processes may be related to Fermi-jets [40], i.e. nucleons accelerated by the action of the mean field and emitted without significant nucleon-nucleon collisions. However, because of the semiclassical nucleonic momentum distribution used in our calculations, the predicted correlations may not be reliable for the highest momenta, $P > 1000$ MeV/c, and should be viewed with caution. In any case, the calculations clearly indicate that one should be able to extract a wealth of information about the space-time evolution of the reaction zone by detailed investigations of the momentum and impact parameter dependence of two-proton correlation functions. Previous measurements of two-particle correlation functions did not determine the simultaneous dependence on impact parameter and momentum of the emitted particle pair and thus averaged over valuable information. New measurements capable of determining such dependences are clearly desirable.

6. *Evaporative Emission*

Correlation functions for particle evaporation from long-lived compound nuclei can be calculated by using the Wigner-function formalism [14] outlined in Section 2. We have used the statistical model of ref. [25] to construct Wigner functions for evaporative emission from equilibrated compound nuclei. In this model, the average particle emission is calculated from a generalized Weisskopf formula and cooling of the compound nucleus is calculated from the average mass and energy emission rates [25].

This generalized Weisskopf formula [25] gives the probability per unit time and energy intervals of emitting a particle, b, with energy, E, at time, t, from a compound nucleus, c:

$$\frac{d^2N_b}{dEdt} = (2S_b+1)\left[\frac{m_b \pi R_b^2}{\pi^2 \hbar^3}\right](E-V_b)\theta(E-V_b)\exp\left[\frac{-E+Z_b F(T,\rho_\pi)+N_b F(T,\rho_\nu)-B_b}{T}\right] . \qquad (44)$$

Here, S_b, m_b, Z_b, N_b, and E denote the spin, mass, charge, neutron number, and energy of the emitted particle; T is the temperature of the compound nucleus; $F(T,\rho_\pi)$ and $F(T,\rho_\nu)$ are the Helmholtz free energies per particle for protons and neutrons, respectively, and $\theta(x)$ is the unit step function. The free energies were calculated by assuming that the nucleons behaved like an ideal Fermi gas with a density of $\rho=0.145$ fm^{-3}. The height of the Coulomb barrier, V_b, was taken as the Coulomb energy between the daughter nucleus and the emitted fragment when they are separated by the absorption radius, R_b. For simplicity, the absorption radius was calculated as:

$$R_b = r_0[(A_c-A_b)^{1/3}+A_b^{1/3}] \; ; \; r_0 = 1.2 \text{ fm} . \qquad (45)$$

Here, A_c and A_b denote the mass numbers of the parent nucleus, c, and the emitted particle, b, respectively. The binding energy, B_b, is the difference in masses of the parent nucleus and that of the daughter nucleus and the emitted particle. The masses of parent and daughter nuclei were calculated from a liquid-drop formula:

$$M(A,Z) = Zm_p c^2+(A-Z)m_n c^2-[14.1A-13A^{2/3}-0.595Z^2A^{-1/3}-19(A-2Z)^2/A]\cdot\text{MeV} . \qquad (46)$$

The spatial distribution of emission points was chosen to be uniform in the two coordinates transverse to the velocity of the emitted particles; the third coordinate was chosen such that the emission point corresponds to the surface of the sphere of radius R_b. For particles with energies very near the Coulomb barrier, this is not a particularly satisfying choice. These particles undergo a significant change in their trajectory due to the Coulomb field of the compound nucleus. Distortions of two-proton correlation functions by deflections of the emitted protons in the Coulomb field of the daughter nucleus are manifestations of long range three-body effects. Such effects are not incorporated in the formalism presented in Section 2. We also neglected effects due to angular momentum coupling which, for rapidly rotating compound nuclei, could modify the extracted radii by up to 20% [19].

If the spatial separation between emitted protons is much larger than the two-proton Bohr radius of 58 fm, one can not only neglect the identical-particle interference of the emitted protons and their strong mutual interaction, but also the quantum nature of their mutual Coulomb repulsion. Under these conditions, one can calculate correlation functions from the classical Coulomb trajectories, where the electric field of both protons and that of the compound nucleus are taken into account [17]. For compound nuclei with excitation energies below about 2.0 MeV/nucleon, emission times scales are sufficiently large that the above conditions are satisfied; classical trajectory calculations should provide a good approximation.

For increasingly high excitation energies, the time scales for emission become shorter. As the protons are emitted closer to one another, the quantum nature of the Coulomb interaction, identical particle statistics, and the strong interaction become important in that order. Fortunately, Coulomb deflections in the field of the compound nucleus become less important for particles emitted with kinetic energies significantly above the Coulomb barrier. For collisions with sufficient energy to dissolve the nuclei, $E/A \gtrsim 50$ MeV, the neglect of three-body effects for the two-proton relative wave function should provide a good approximation. At these energies, the effects of the strong interaction and identical particle interactions dominate. These effects can only be calculated by a full quantum treatment of the relative wave function.

7. Numerical calculations

It is instructive to explore the sensitivity of the calculated correlation functions to various parameters and momentum cuts. The following illustrative calculations are performed for narrow ranges of the total momenta, $P_{c.m.}$, of the emitted particle pairs. (The momenta, $P_{c.m.}$, are defined with respect to the compound nucleus rest frame.)

The shape of the two-proton correlation function depends on the time-scale governing the emission of the detected particles. For particle emission from equilibrated compound nuclei, this time scale depends on the level density and, therefore, on the initial temperature. Because of cooling via particle emission, the time scale also depends on the energy of the emitted particles. In Figs. 14 and 15, such dependences are illustrated for the decay of highly excited ^{156}Ho nuclei. Figure 14 shows the calculated time dependence of the respective emission processes, i.e. the relative probability per unit time for the emission of the specified protons. The predicted two-proton correlation functions are shown in Fig. 15. The top panels in the two figures present calculations for initial temperatures T = 5, 10, and 20 MeV, keeping the total momentum of the two-proton pair fixed at $P_{c.m.}$=400±10 MeV/c. (This momentum bin selects protons of kinetic energy $E_{c.m.}/A \approx 21$ MeV in the compound nucleus rest frame.) At low temperatures, $T \lesssim 5$ MeV, the decay times are large and the predicted correlation functions exhibit only a minimum at q≈0 MeV/c. With increasing temperature, the decay times decrease and the minimum at q=0 MeV becomes more pronounced. For very hot nuclear systems, $T \gtrsim 20$ MeV, the calculated emission time scales become so short that the two-proton nuclear interaction becomes significant and the maximum in the correlation function at q≈20 MeV/c emerges. The bottom panels of Figs. 14 and 15 show calculations for different total momenta, $P_{c.m.}$, and fixed initial temperature, T=10 MeV. Because of cooling of the compound nucleus, particles of higher energy are emitted on faster time-scales than particles of lower energy. As a consequence, the two-proton correlation functions reflect smaller apparent source dimensions for the emission of particles of increasing energy. At lower temperatures, qualitatively similar dependences exist, but their effects on the two-proton correlation functions are less visible due to the larger emission times.

For fixed excitation energy, E*, the decay rate of a compound nucleus depends on the relation between excitation energy and temperature since higher temperatures lead to higher emission rates and, therefore, to smaller apparent source dimensions. Figure 16 illustrates the sensitivity of the calculated two-proton correlation functions to the assumed relation between excitation energy and temperature for the decay of ^{156}Ho compound nuclei of fixed initial excitation energy, E*/A=6.0 MeV. In these calculations, the level density was taken as that of an ideal Fermi-gas of the indicated spatial density ρ. For an ideal Fermi gas, the relation between excitation energy and temperature is given to first order by

$$T^2 = E^*/a \ . \tag{47}$$

The level density parameter, a, depends on the Fermi energy, ε_F:

$$a = \frac{\pi^2 A}{4\varepsilon_F} \approx 0.065A\{\rho_0/\rho\}^{2/3} \ \text{MeV}^{-1}. \tag{48}$$

In Eq. (48), we have used the relation $\varepsilon_F \approx 38(\rho/\rho_0)^{2/3}$ MeV, where $\rho_0 \approx 0.17$ fm^{-3} denotes the density of normal nuclear matter. For reference, the level density parameters are also indicated in Fig. 16. The calculations indicate only a moderate sensitivity to the level density parameter. As expected, higher temperatures produce shorter emission times and, hence, more pronounced correlations.

Particle emission rates depend largely upon the temperature of the compound nucleus. Yet, the initial temperature does not specify the decay characteristics unambiguously, because different level density parameters represent different heat capacities of the decaying nuclear system. Figure 17 shows the sensitivity of the calculated two-proton correlation functions to the level density parameter for ^{156}Ho compound nuclei of fixed initial temperature, T=10 MeV. The predicted correlations are slightly more attenuated for larger level density parameters, i.e. for increasing values of the heat capacity of the compound nucleus. However, the sensitivity is not very pronounced; it is even less significant at lower temperatures.

Since the predicted emission times depend strongly on the momenta of the emitted particles, the differences between longitudinal and transverse correlation functions can be expected to be momentum-dependent. Low energy particles may be emitted on such long time-scales that sensitivity to antisymmetrization effects is lost. As emission time scales decrease for more energetic emissions, differences between longitudinal and transverse correlation functions may become more significant for particle pairs of higher total momenta. These qualitative expectations are corroborated by the calculations shown in Fig. 18. The solid and dashed curves show longitudinal and transverse correlation functions predicted for narrow gates on the total momentum, $P_{c.m.}$ = 300, 400, 500 MeV/c, of the particle pair with respect to the center-of-mass frame of reference (i.e. the rest frame of the compound nucleus). Significant differences between longitudinal and transverse correlation functions are predicted for large momenta, P=500 MeV/c (top panel). These differences are reduced for smaller momenta, $P_{c.m.}$=400 MeV/c (center panel). For even smaller momenta, $P_{c.m.}$=300 MeV/c, longitudinal and transverse correlation functions differ only in the detailed shape of the minimum at q≈0 MeV/c (bottom panel) which is more pronounced for the longitudinal than for the transverse correlation function.

8. *Summary and conclusion*

We have presented a general formalism allowing the calculation of two-proton correlation functions for any reaction model capable of predicting the one-body phase-space distribution of the emitted particles. We demonstrated the sensitivity of two-proton correlation functions to the space-time geometry of the emitting system via calculations for schematic emission sources, as well as for more realistic models of compound and precompound light particle emissions.

Particle emission from equilibrated compound nuclei typically proceeds on such long time scales that antisymmetrization and nuclear interaction between the two emitted particles play a relatively minor role. The correlation functions are dominated by final state Coulomb interactions and exhibit only moderate sensitivity to details of the calculations. Once emission times are of the order of 100 fm/c or less, antisymmetrization effects, nuclear and Coulomb interactions must all be incorporated into the calculations and the

correlation functions become rather sensitive to details of the space-time evolution of the reaction zone. The BUU calculations indicate considerable sensitivity of the predicted correlation functions to the magnitude of the in-medium nucleon-nucleon cross sections employed in these calculations. Small differences are predicted between transverse and longitudinal correlation functions which could be explored for further testing of reaction models. Considerable sensitivity is predicted for measurements which explore the dependence of the two-proton correlation function on the collision impact parameter and on the total momenta of the emitted proton pairs.

The authors would like to acknowledge helpful discussions with G.J. Kunde. This work is based upon work supported by the National Science Foundation under Grant numbers PHY-89-13813, PHY-89-06116, and PHY-88-1439. S.P. gratefully acknowledges additional support from the Wisconsin Alumni Research Foundation and from the NSCL.

References

1. For a recent review, see e.g. D.H. Boal, C.K. Gelbke, and B.K. Jennings, Rev. Mod. Phys. 62, 553 (1990).
2. S.E. Koonin, Phys. Lett. 70B, 43 (1977).
3. F. Zarbakhsh, A.L. Sagle, F. Brochard, T.A. Mulera, V. Perez-Mendez, R. Talaga, I. Tanihata, J.B. Carroll, K.S. Ganezer, G. Igo, J. Oostens, D. Woodard, and R. Sutter, Phys. Rev. Lett. 46, 1268 (1981).
4. W.G. Lynch, C.B. Chitwood, M.B. Tsang, D.J. Fields, D.R. Klesch, C.K. Gelbke, G.R. Young, T.C. Awes, R.L. Ferguson, F.E. Obenshain, F. Plasil, R.L. Robinson and A.D. Panagiotou, Phys. Rev. Lett. 51, 1850 (1983).
5. H.A. Gustafsson, H.H. Gutbrod, B. Kolb, H. Löhner, B. Ludewigt, A.M. Poskanzer, T. Renner, H. Riedesel, H.G. Ritter, A. Warwick, F. Weik, and H. Wieman, Phys. Rev. Lett. 53, 544 (1984).
6. C.B. Chitwood, J. Aichelin, D.H. Boal, G. Bertsch, D.J. Fields, C.K. Gelbke, W.G. Lynch, M.B. Tsang, J.C. Shillcock, T.C. Awes, R.L. Ferguson, F.E. Obenshain, F. Plasil, R.L. Robinson, and G.R. Young, Phys. Rev. Lett. 54, 302 (1985).
7. B.K. Jennings, D.H. Boal, and J.C. Shillcock, Phys. Rev. C33, 1303 (1986).
8. D.H. Boal and J.C. Shillcock, Phys. Rev. C33, 549 (1986).
9. C.B. Chitwood, C.K. Gelbke, J. Pochodzalla, Z. Chen, D.J. Fields, W.G. Lynch, R. Morse, M.B. Tsang, D.H. Boal, and J.C. Shillcock, Phys. Lett. 172B, 27 (1986).
10. Z. Chen, C.K. Gelbke, J. Pochodzalla, C.B. Chitwood, D.J. Fields, W.G. Lynch and M.B. Tsang, Phys. Lett. B186, 280 (1987).
11. Z. Chen, C.K. Gelbke, W.G. Gong, Y.D. Kim, W.G. Lynch, M.R. Maier, J. Pochodzalla, M.B. Tsang, F. Saint-Laurent, D. Ardouin, H. Delagrange, H. Doubre, J. Kasagi, A. Kyanowski, A. Péghaire, J. Péter, E. Rosato, G. Bizard, F. Lefèbvres, B. Tamain, J. Québert, and Y.P. Viyogi, Phys. Rev. C36, 2297 (1987).
12. J. Pochodzalla, C.K. Gelbke, W.G. Lynch, M. Maier, D. Ardouin, H. Delagrange, H. Doubre, C. Grégoire, A. Kyanowski, W. Mittig, A. Péghaire, J. Péter, F. Saint-Laurent, B. Zwieglinski, G. Bizard, F. Lefèbvres, B. Tamain, and J. Québert, Y.P. Viyogi, W.A. Friedman, and D.H. Boal, Phys. Rev. C35, 1695 (1987).

13. J. Pochodzalla, C.B. Chitwood, D.J. Fields, C.K. Gelbke, W.G. Lynch, M.B. Tsang, D.H. Boal, and J.C. Shillcock, Phys. Lett. B174, 36 (1986).
14. S. Pratt and M.B. Tsang, Phys. Rev. C36, 2390 (1987).
15. D. Fox, D.A. Cebra, J. Karn, C. Parks, A. Pradhan, A. Vander Molen, J. van der Plicht, G.D. Westfall, W.K. Wilson, and R.S. Tickle, Phys. Rev. C38, 146 (1988).
16. T.C. Awes, R.L. Ferguson, F.E. Obenshain, F. Plasil, G.R. Young, S. Pratt, Z. Chen, C.K. Gelbke, W.G. Lynch, J. Pochodzalla, and H.M. Xu, Phys. Rev. Lett. 61, 2665 (1988).
17. P.A. DeYoung, M.S. Gordon, Xiu qin Lu, R.L. McGrath, J.M. Alexander, D.M. de Castro Rizzo, and L.C. Vaz, Phys. Rev. C39, 128 (1989).
18. D.A. Cebra, W. Benenson, Y. Chen, E. Kashy, A. Pradhan, A. Vander Molen, G.D. Westfall, W.K. Wilson, D.J. Morrissey, R.S. Tickle, R. Korteling, and R.L. Helmer, Phys. Lett. B227, 336 (1989).
19. S.E. Koonin, W. Bauer, and A. Schäfer, Phys. Rev. Lett. 62, 1247 (1989).
20. J. Québert, R. Boisgard, P. Lautridou, D. Ardouin, D. Durand, D. Goujdami, F. Guilbault, C. Lebrun, R. Tamisier, A. Péghaire, and F. Saint-Laurent, Proceedings of the Symposium on Nuclear Dynamics and Nuclear Disassembly, held at Dallas, April 1989, edited by J.B. Natowitz, World Scientific, Singapore 1989, p. 337.
21. D. Ardouin, F. Guilbault, C. Lebrun, D. Ardouin, S. Pratt, P. Lautridou, R. Boisgard, J. Québert, and A. Péghaire, University of Nantes, Internal Report LPN-89-02.
22. P.A. DeYoung, C.J. Gelderloos, D. Kortering, J. Sarafa, K. Zienert, M.S. Gordon, B.J. Fineman, G.P. Gilfoyle, X. Lu, R.L. McGrath, D.M. de Castro Rizzo, J.M. Alexander, G. Auger, S. Kox, L.C. Vaz, C. Beck, D.J. Henderson, D.G. Kovar, and M.F. Vineyard, Phys. Rev. C41, R1885 (1990).
23. W.G. Gong, C.K. Gelbke, N. Carlin, R.T. de Souza, Y.D. Kim, W.G. Lynch, T. Murakami, G. Poggi, D. Sanderson, M.B. Tsang, H.M. Xu, D.E. Fields, K. Kwiatkowski, R. Planeta, V.E. Viola, Jr., S.J. Yennello, and S. Pratt, Phys. Lett. B246, 21 (1990).
24. W.G. Gong, C.K. Gelbke, N. Carlin, R.T. de Souza, Y.D. Kim, W.G. Lynch, T. Murakami, G. Poggi, D. Sanderson, M.B. Tsang, H.M. Xu, D.E. Fields, K. Kwiatkowski, R. Planeta, V.E. Viola, Jr., S.J. Yennello, and S. Pratt, to be published in Phys. Rev. C.
25. W.A. Friedman and W.G. Lynch, Phys. Rev. C28, 16 (1983).

26. D.H. Boal and H. DeGuise, Phys. Rev. Lett. 57, 2901 (1986).
27. S. Pratt, Phys. Rev. Lett. 53, 1219 (1984).
28. A. Messiah, Quantum Mechanics, Vol. 1 (Appendix), North Holland Publishing Company, Amsterdam (1976).
29. R.V. Reid, Jr., Ann. Phys. (N.Y.) 50, 411 (1968).
30. L.W. Nordheim, Proc. Roy. Soc. A119, 689 (1928).
31. C.Y. Wong, Phys. Rev. C25, 1460 (1982).
32. M.B. Tsang, W.G. Lynch, C.B. Chitwood, D.J. Fields, D.R. Klesch, C.K. Gelbke, G.R. Young, T.C. Awes, R.L. Ferguson, F. E. Obenshain, F. Plasil, and R.L. Robinson, Phys. Lett. 148B, 265 (1984).
33. C.B. Chitwood, D.J. Fields, C.K. Gelbke, D.R. Klesch, W.G. Lynch, M.B. Tsang, T.C. Awes, R.L. Ferguson, F.E. Obenshain, F. Plasil, R.L. Robinson, and G.R. Young, Phys. Rev. C34, 858 (1986).
34. W. Bauer, Nucl. Phys. A471, 604 (1987).
35. W. Bauer, G.D. Westfall, D. Fox, and D. Cebra, Phys. Rev. C37, 664 (1988).
36. D. Ardouin, Z. Basrak, P. Schuck, A. Péghaire, F. Saint-Laurent, H. Delagrange, H. Doubre, C. Grégoire, A. Kyanowski, W. Mittig, J. Péter, Y.P. Viyogi, J. Québert, C.K. Gelbke, W.G. Lynch, M. Maier, J. Pochodzalla, G. Bizard, F. Lefèbvres, B. Tamain, B. Remaud, and F. Sébille, Nucl. Phys. A514, 564 (1990).
37. G.F. Bertsch, H. Kruse, and S. Das Gupta, Phys. Rev. C29, 673 (1984).
38. G.F. Bertsch and S. Das Gupta, Phys. Rep. 160, 189 (1988).
39. A detailed account of the numerical details is given in W. Bauer, Michigan State University report MSUCL-699, submitted to Phys. Rev. C.
40. J.P. Bondorf, J.N. De, G. Fai, A.O.T. Karvinen, B. Jacobsson, and J. Randrup, Nucl. Phys. A333, 285 (1980).

Figure Captions:

Fig. 1. Two-proton correlation functions calculated for short-lived Gaussian sources of representative radius parameters, r_0=2.5, 5, 10, 20 fm. The solid curves show the result of the full calculations; the dotted curves show calculations for which the nuclear interaction is neglected; the dashed curves shown calculations for which the nuclear interaction and the Pauli principle are neglected.

Fig. 2. Two proton correlation functions calculated for sources of negligible lifetime assuming Gaussian (solid lines) and sharp sphere (dotted lines) density distributions. The radius parameters, r_0 and R_s, are indicated.

Fig. 3. Relation between radius parameters, r_0 and R_s, of Gaussian and sharp sphere density distributions for which equivalent two-proton correlation functions are obtained in the limit of negligible lifetime. Crosses indicate results of numerical calculations, the solid line represents a linear fit, and the dotted curve shows the relation $R_s=(5/2)^{1/2}r_0$ used in the literature [1].

Fig. 4. Two-proton correlation functions predicted for emission from spherical sources of radius R_s=5 fm, decaying isotropically with fixed life-time, Eq. (27). The top and bottom panels depict the dependence on life-time, τ, and total momentum, $P_{c.m.}$, respectively.

Fig. 5. Longitudinal and transverse correlation functions calculated for emission from sources decaying with constant lifetimes, Eq. (27). The parameters used in these calculations are indicated in the figure.

Fig. 6. Dependence of correlation functions predicted by BUU calculations on the emission time intervals, Δt_e, and the emission densities, ρ_e. The values of individual parameter choices and selected total momenta of the proton pairs are given in the figure. In these calculations, the in-medium cross section was approximated by the experimental free nucleon-nucleon cross section, and the stiff equation of state was used.

Fig. 7. Sensitivity of two-proton correlation functions to the nuclear equation of state (EOS) and the in-medium nucleon-nucleon cross section. Different panels show results calculated for different total momenta, P, of the proton pairs.

Fig. 8. Comparison of two-proton correlation functions predicted for different source geometries: the solid points represent the results of BUU calculations averaged over the momentum range P=450-780 MeV/c. The curves show emission from sources of negligible lifetime: the solid and dashed curves are obtained, respectively, for a spherical Gaussian source of radius parameter, r_0=4.5 fm, and a source consisting of two sharp spheres of radius, R_s=5 fm, and separated by the distance, d=20 fm.

Fig. 9. Nucleon density distributions in the reaction plane calculated from the BUU equation for $^{14}N+^{27}Al$ collisions at E/A=75 MeV and for an impact parameter of b=2 fm. Different panels depict the distributions at different times, t.

Fig.10. Spatial distributions of emitted nucleons in the reaction plane calculated from the BUU equation for $^{14}N+^{27}Al$ collisions at E/A=75 MeV and for an impact parameter of b=2 fm. Different panels depict the distributions at different times, t.

Fig.11. Longitudinal, and transverse correlation functions predicted by BUU calculations for $^{14}N+^{27}Al$ collisions at E/A=75 MeV for particle pairs for the indicated total momenta, P.

Fig.12. Two-proton correlation functions predicted by BUU calculations for $^{14}N+^{27}Al$ collisions at E/A=75 MeV for the indicated impact parameters and total momenta of the emitted proton pairs.

Fig.13. Momentum dependence of the heights of the maxima of two-proton correlation functions predicted by BUU calculations for $^{14}N+^{27}Al$ collisions at different impact parameters. Lines connect points corresponding to a given impact parameter to guide the eye.

Fig.14. Temporal evolution of particle emission from equilibrated ^{156}Ho nuclei of different initial temperatures, T (top panel), and for different total momenta, $P_{c.m.}$ (bottom panel), of the emitted two-proton pairs.

Fig.15. Dependence of two-proton correlation function on the initial temperature, T (top panel), and on the total momentum, $P_{c.m.}$ (bottom panel), of emitted proton pairs calculated for the decay of equilibrated ^{156}Ho nuclei.

Fig.16. Sensitivity of calculated two-proton correlation functions to different assumptions on the level density parameter, $a=E^*/AT^2$, for the decay of ^{156}Ho compound nuclei of initial excitation energy $E^*/A=6$ MeV.

Fig.17. Sensitivity of calculated two-proton correlation functions to different assumptions on the level density parameter, $a=E^*/AT^2$, for the decay of ^{156}Ho compound nuclei of initial temperature T=10 MeV.

Fig.18. Longitudinal and transverse correlation functions predicted for evaporative emission from ^{156}Ho compound nuclei of initial temperature, T=10 MeV. Different panels show predictions for different total momenta, $P_{c.m.}$, of the emitted proton pairs: $P_{c.m.}$=500 MeV/c (top panel), $P_{c.m.}$=400 MeV/c (center panel), $P_{c.m.}$=300 MeV/c (bottom panel).

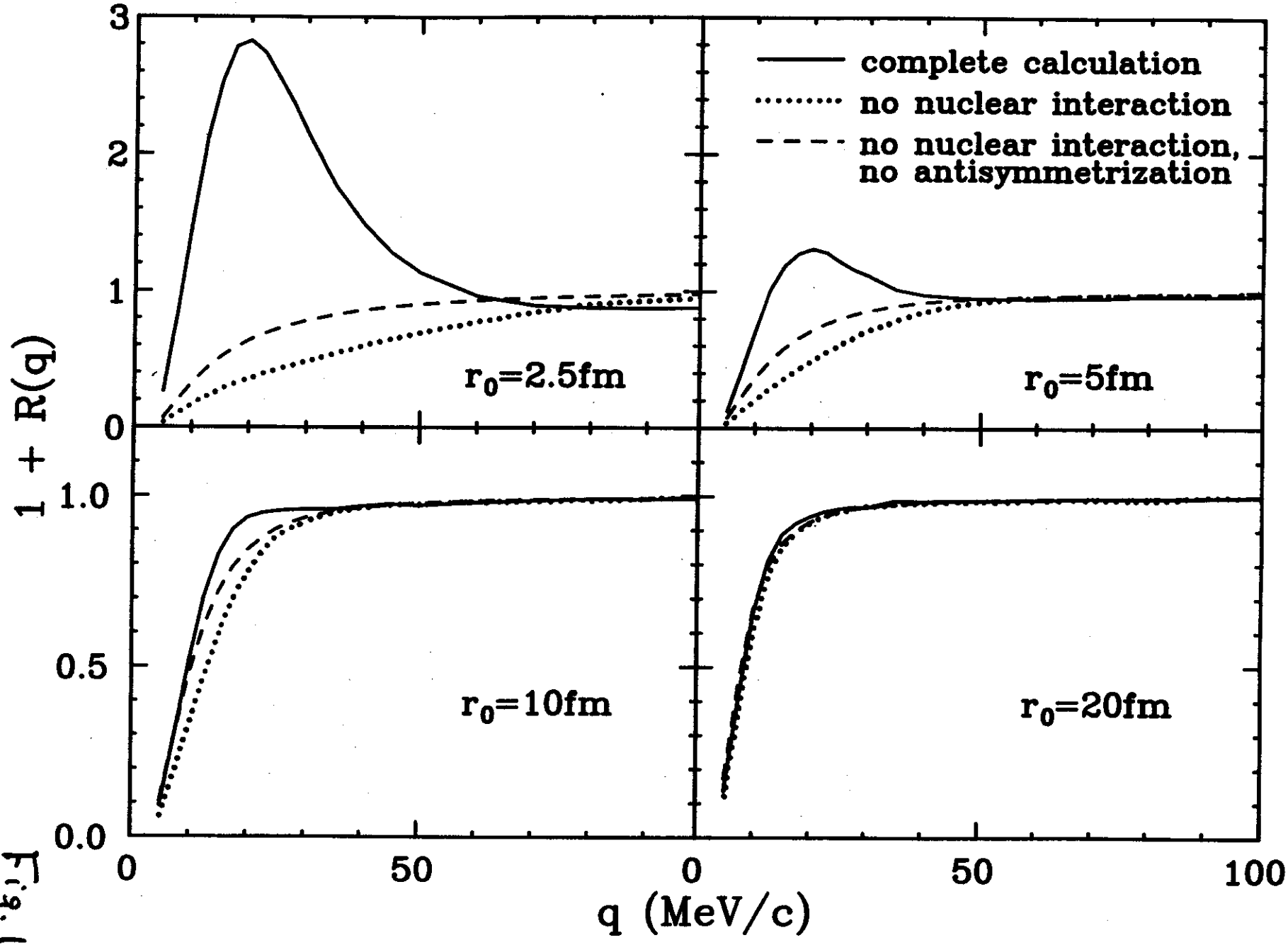
complete calculation
no nuclear interaction
no nuclear interaction, no antisymmetrization
r0=2.5fm
r0=5fm
r0=10fm
r0=20fm
1 + R(q)
q (MeV/c)
0
1
2
3
0.0
0.5
1.0
0
50
0
50
100

Fig. 1

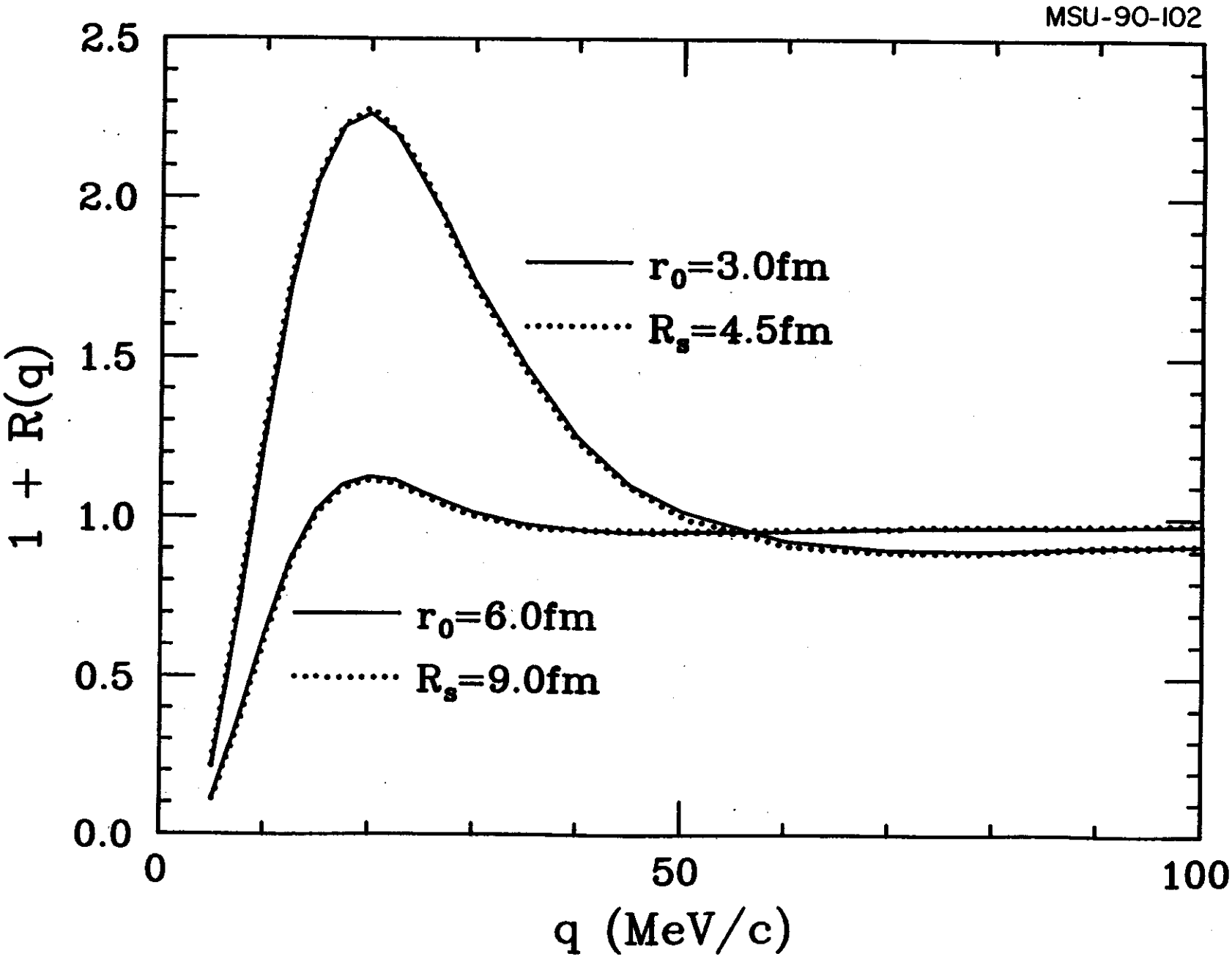
MSU-90-102
2.5
2.0
1.5
1.0
0.5
0.0
1 + R(q)
0
50
100
q (MeV/c)
r0=3.0fm
Rs=4.5fm
r0=6.0fm
Rs=9.0fm

Fig. 2

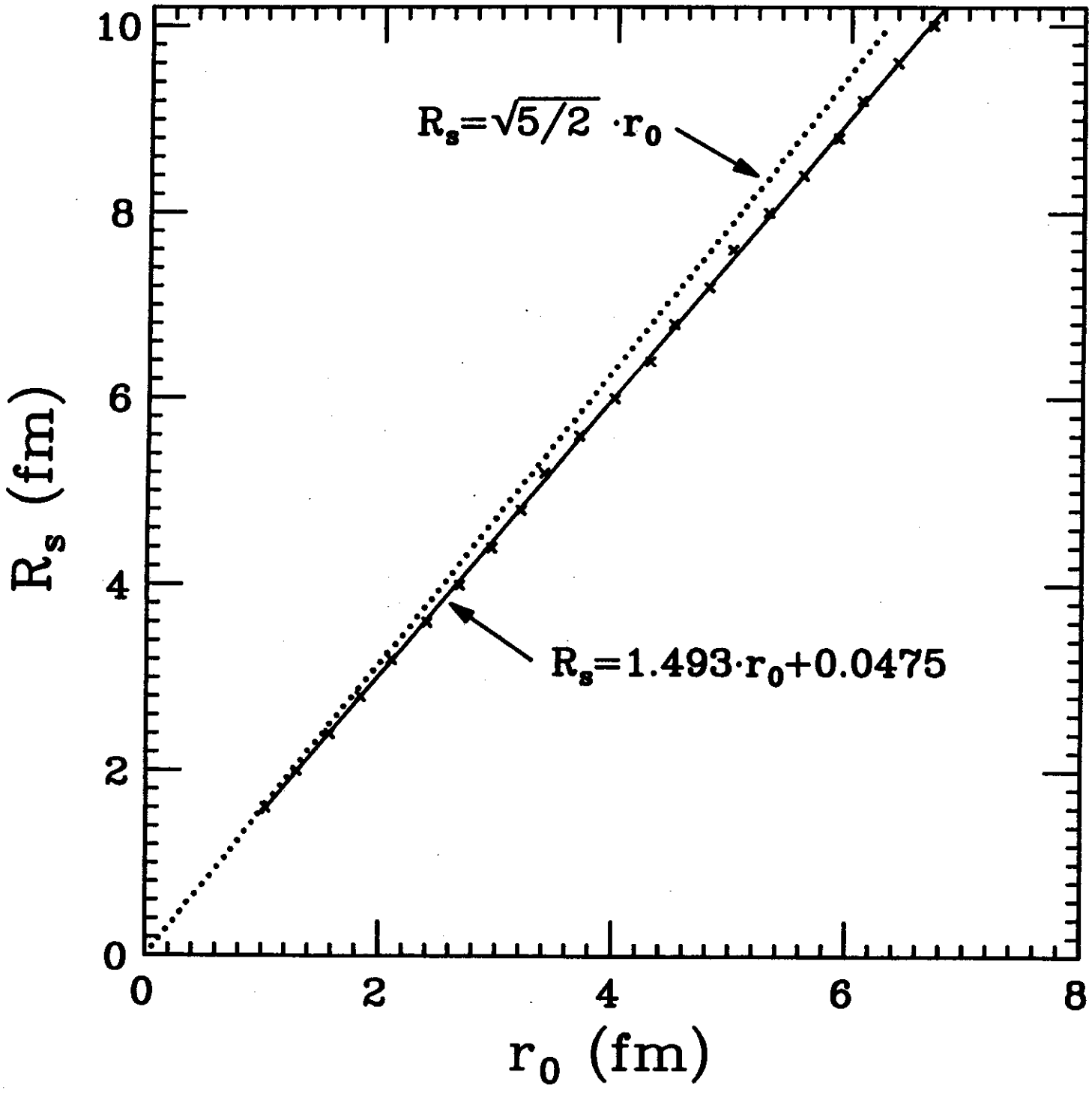

Fig. 3

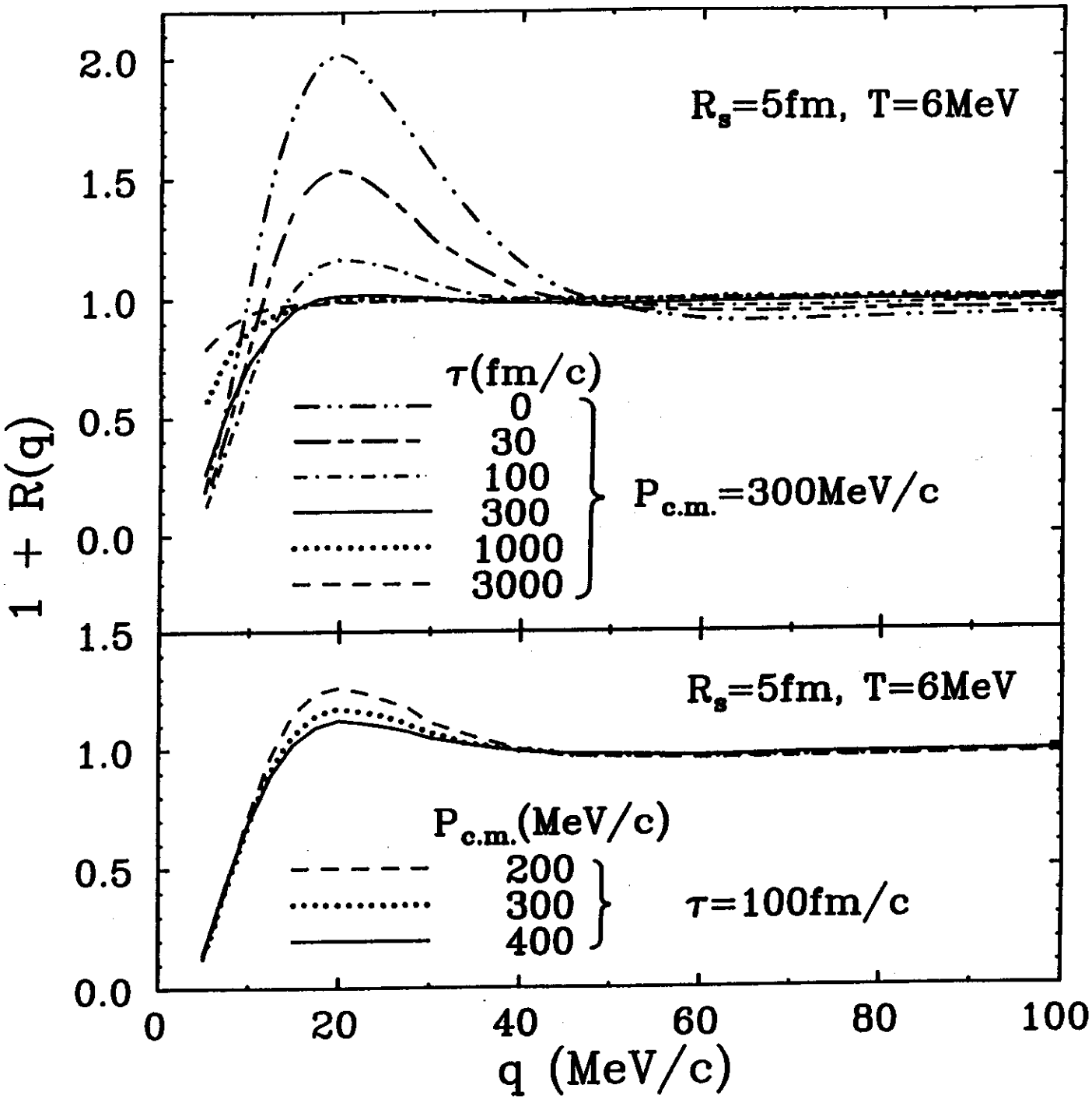
2.0
1.5
1.0
0.5
0.0
1 + R(q)
R_s=5fm, T=6MeV
τ(fm/c)
0
30
100
300
1000
3000
P_c.m.=300MeV/c
1.5
1.0
0.5
0.0
R_s=5fm, T=6MeV
P_c.m.(MeV/c)
200
300
400
τ=100fm/c
0
20
40
60
80
100
q (MeV/c)

Fig. 4

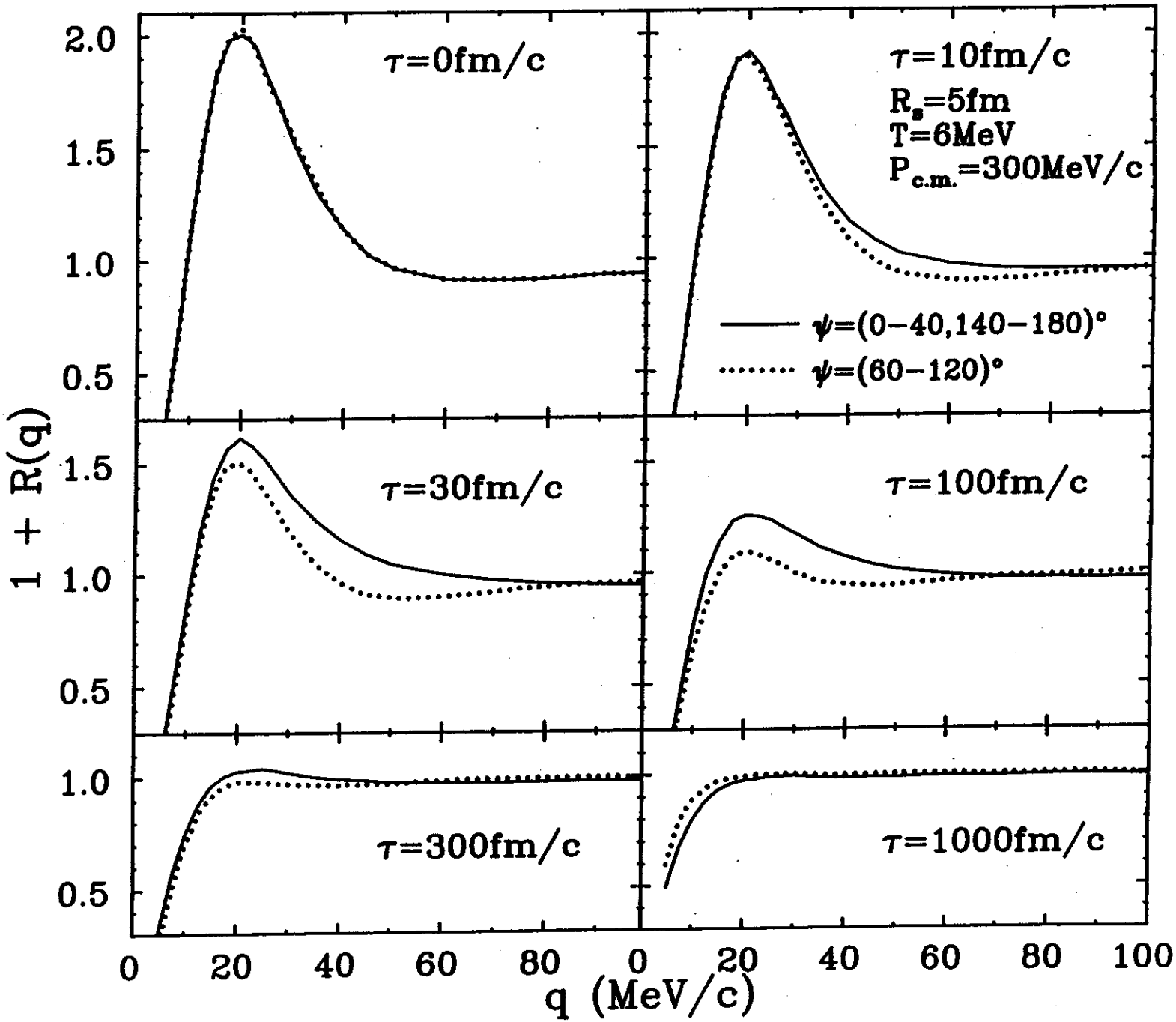
τ=0fm/c
τ=10fm/c
R_s=5fm
T=6MeV
P_c.m.=300MeV/c
ψ=(0−40,140−180)°
ψ=(60−120)°
τ=30fm/c
τ=100fm/c
τ=300fm/c
τ=1000fm/c
1 + R(q)
q (MeV/c)
2.0
1.5
1.0
0.5
0
20
40
60
80
100

Fig 5

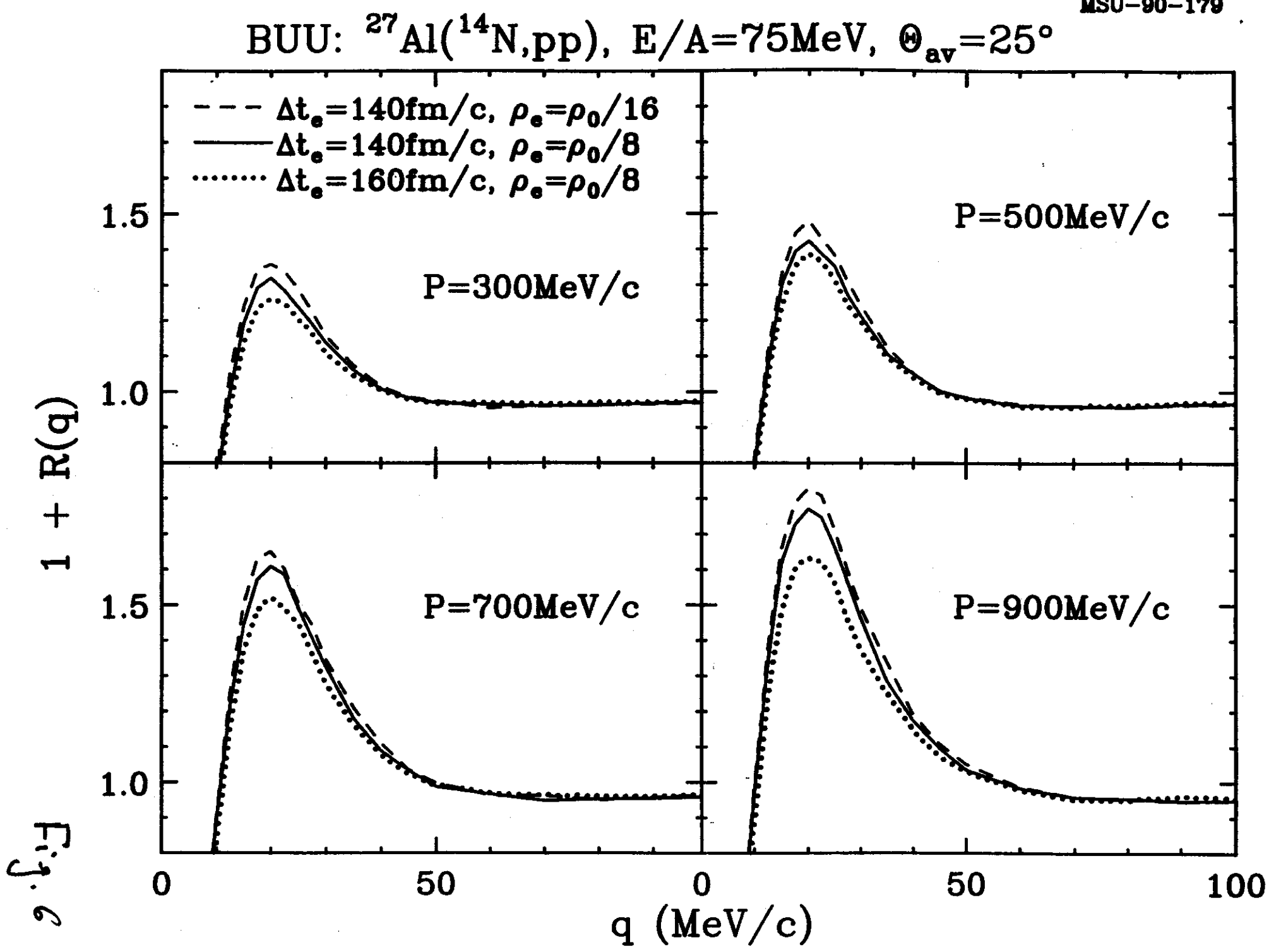
BUU: ^{27}Al(^{14}N,pp), E/A=75MeV, Θ_{av}=25°
Δt_e=140fm/c, $\rho_e=\rho_0/16$
Δt_e=140fm/c, $\rho_e=\rho_0/8$
Δt_e=160fm/c, $\rho_e=\rho_0/8$
P=300MeV/c
P=500MeV/c
P=700MeV/c
P=900MeV/c
1 + R(q)
q (MeV/c)
1.5
1.0
0
50
100

Fig. 6

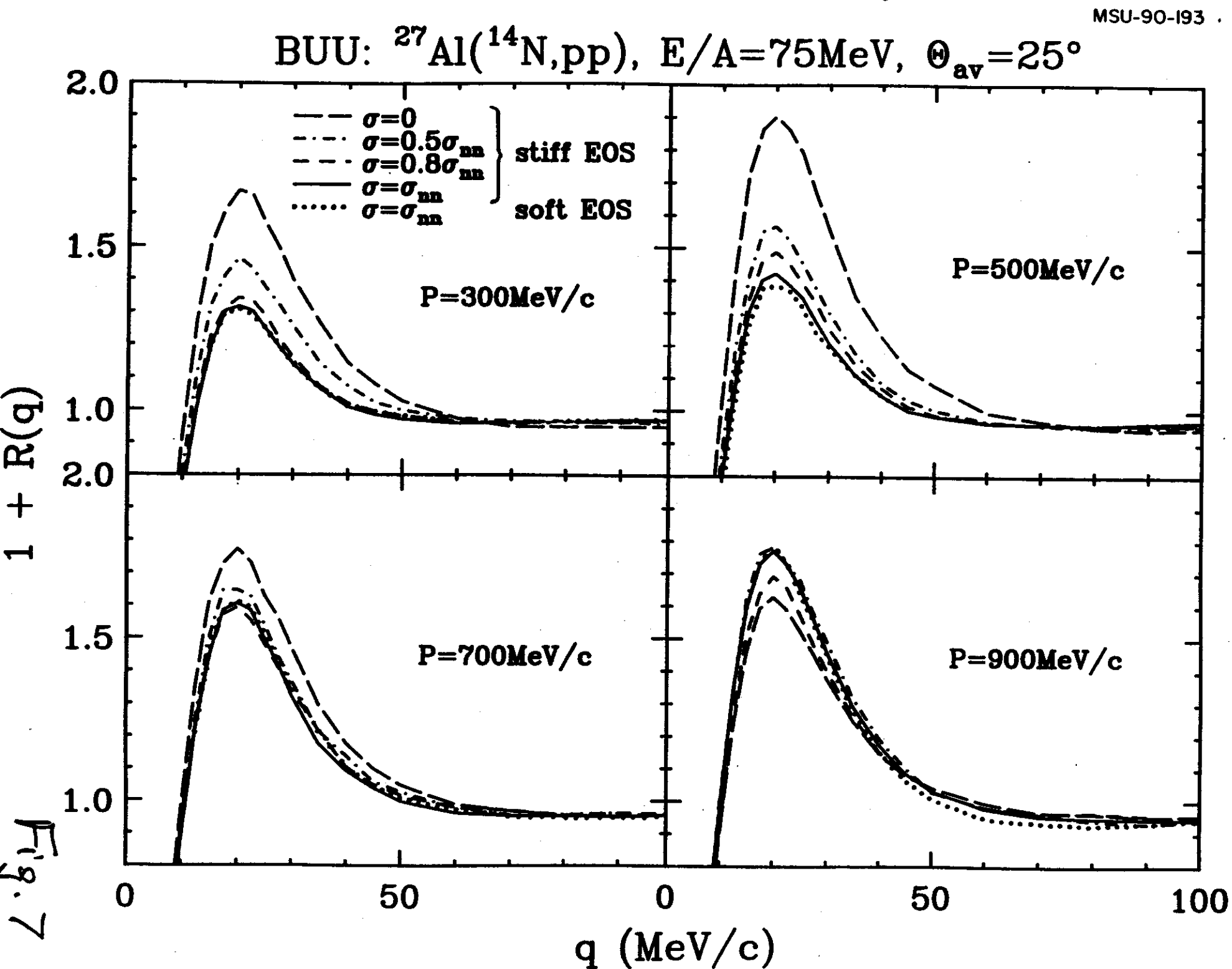
BUU: ^{27}Al(^{14}N,pp), E/A=75MeV, Θ_{av}=25°
σ=0
σ=0.5σ_nn
σ=0.8σ_nn
σ=σ_nn
σ=σ_nn
stiff EOS
soft EOS
P=300MeV/c
P=500MeV/c
P=700MeV/c
P=900MeV/c
1 + R(q)
q (MeV/c)
2.0
1.5
1.0
0
50
100

Fig. 7

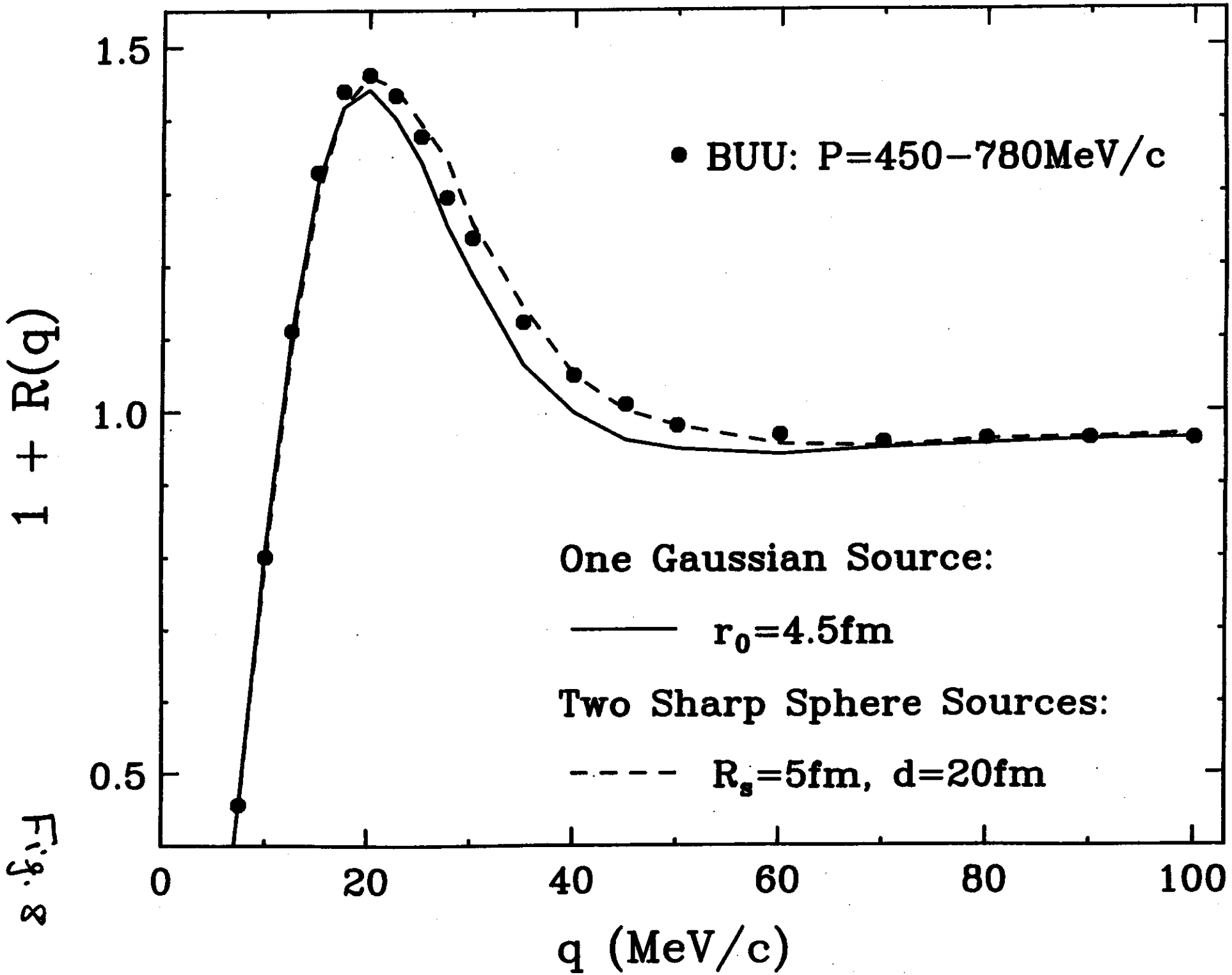
1.5
1.0
0.5
1 + R(q)
0
20
40
60
80
100
q (MeV/c)
• BUU: P=450−780MeV/c
One Gaussian Source:
r_0=4.5fm
Two Sharp Sphere Sources:
R_s=5fm, d=20fm

Fig. 8

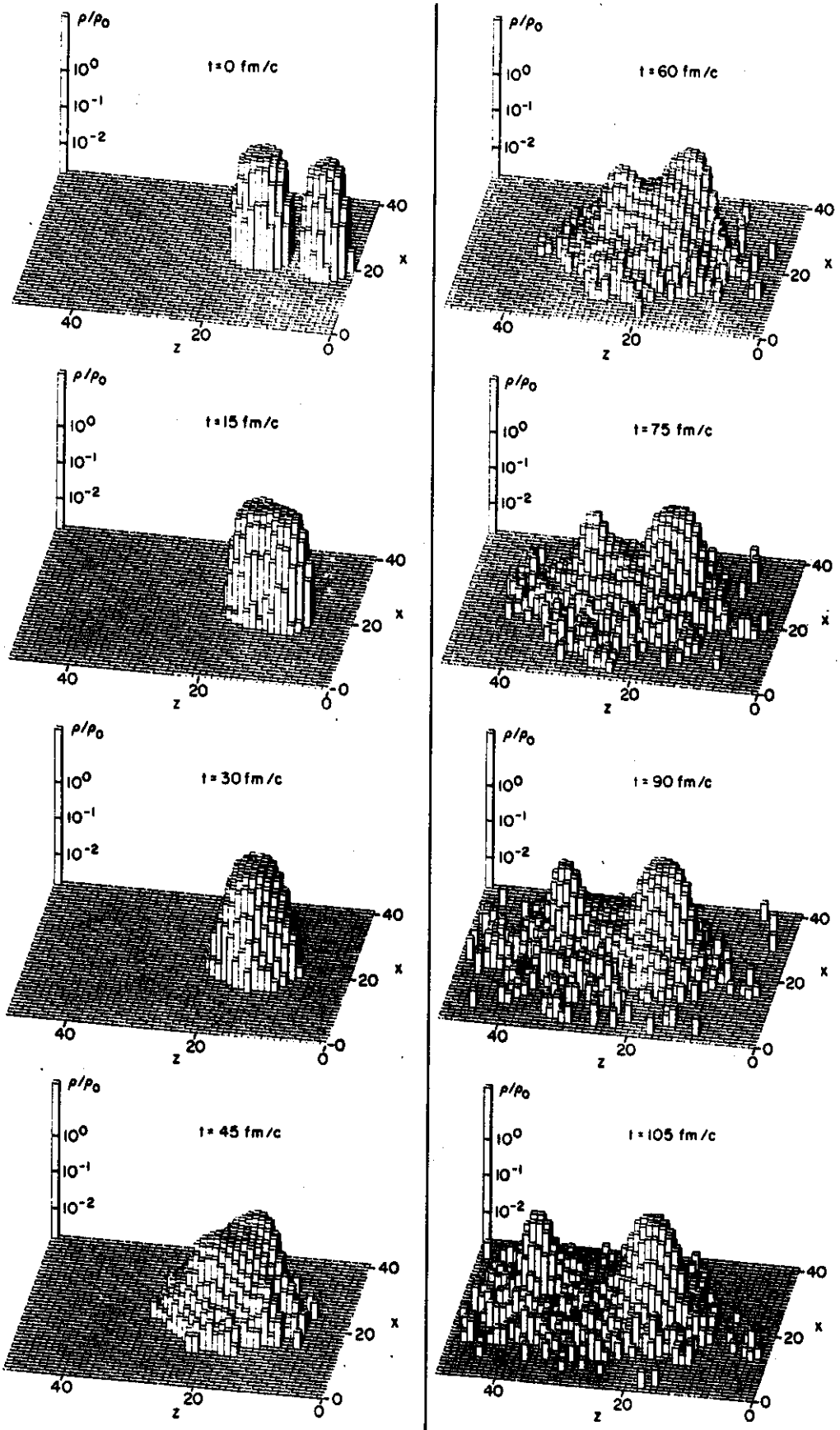
ρ/ρ0
10^0
10^-1
10^-2
t=0 fm/c
t=15 fm/c
t=30 fm/c
t=45 fm/c
t=60 fm/c
t=75 fm/c
t=90 fm/c
t=105 fm/c
40
20
0
z
x

Fig. 9

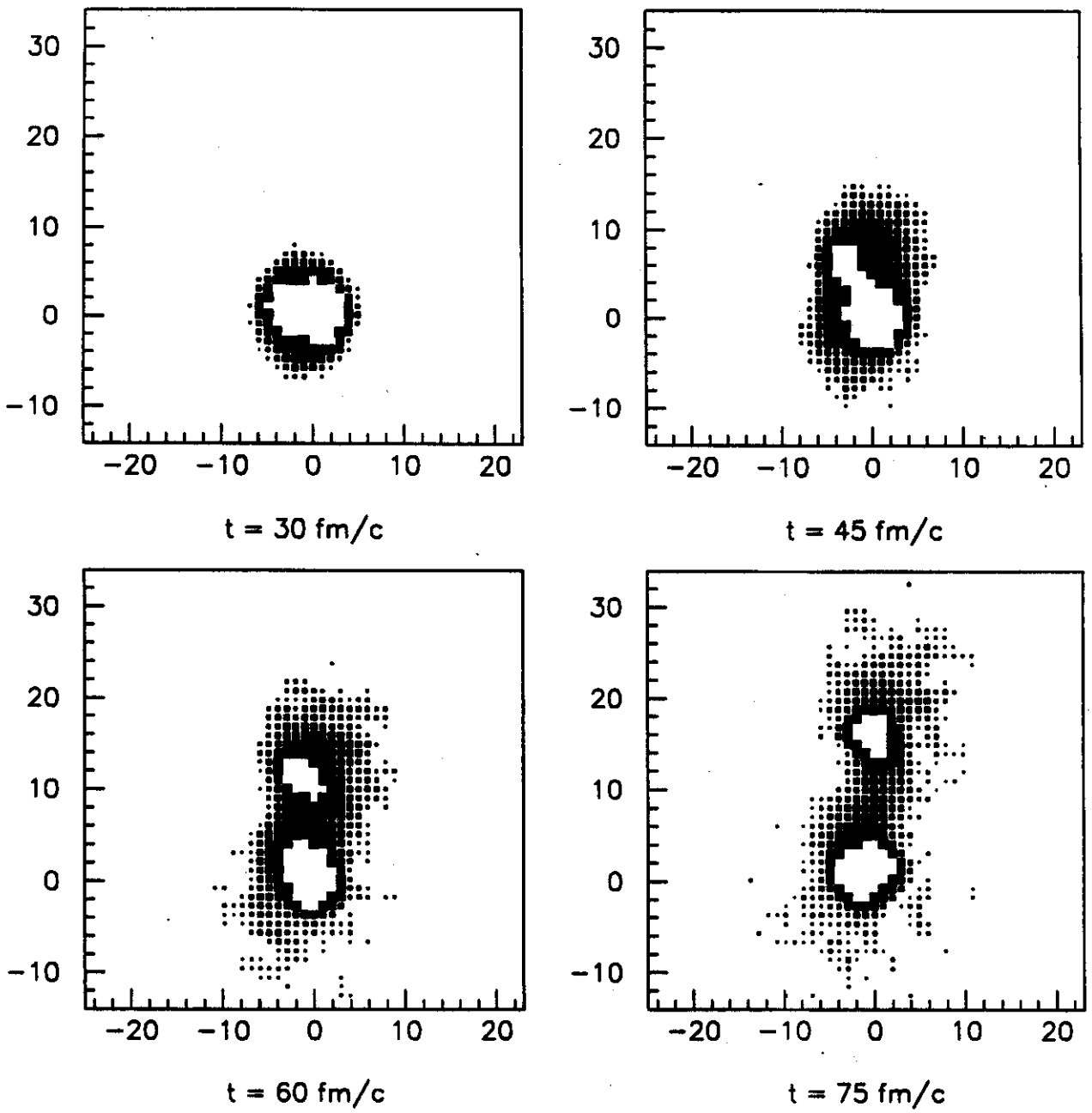

Fig. 10

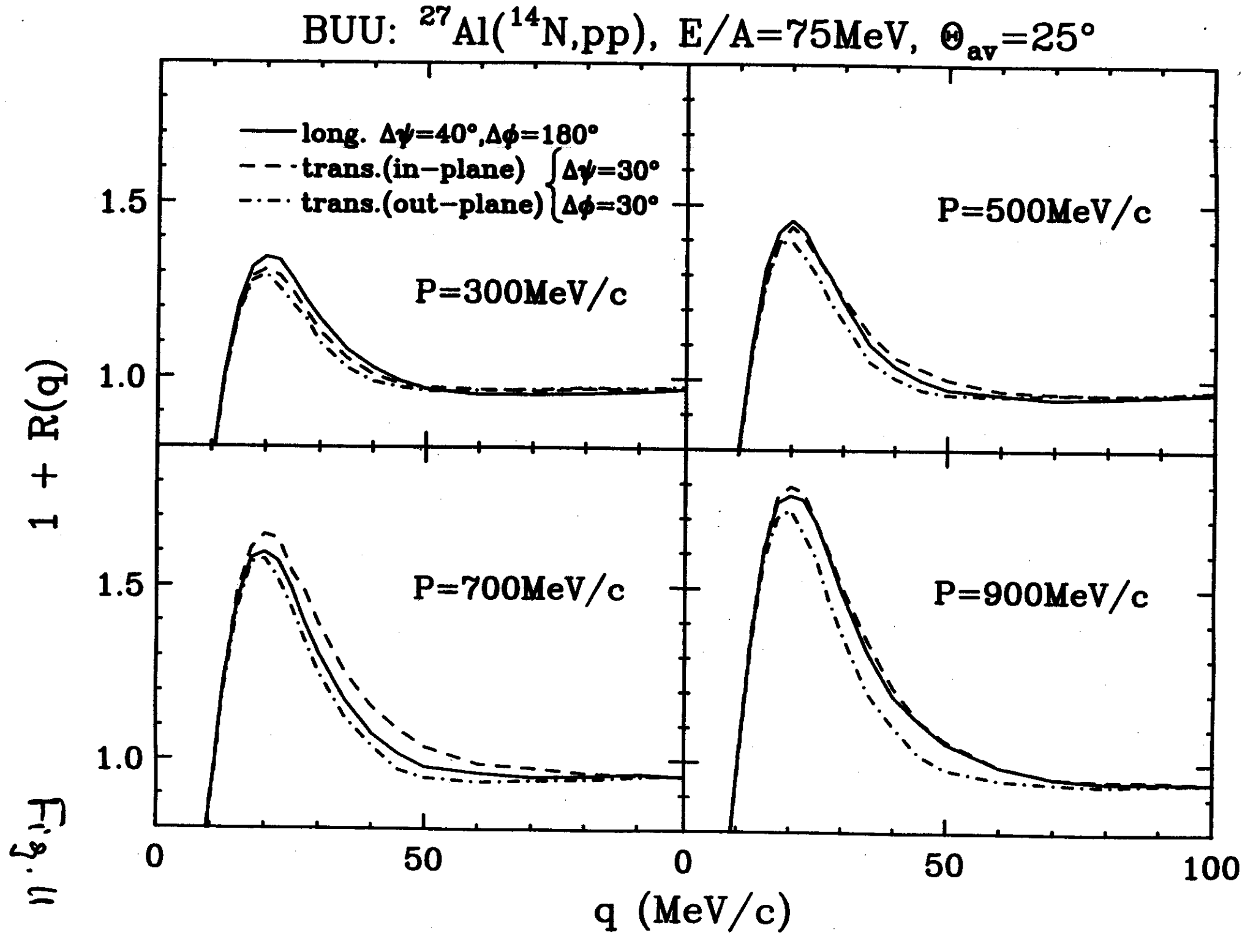
BUU: ^{27}Al(^{14}N,pp), E/A=75MeV, Θ_{av}=25°
long. Δψ=40°,Δφ=180°
trans.(in−plane) Δψ=30°
trans.(out−plane) Δφ=30°
P=300MeV/c
P=500MeV/c
P=700MeV/c
P=900MeV/c
1 + R(q)
q (MeV/c)
1.5
1.0
0
50
100

Fig. 11

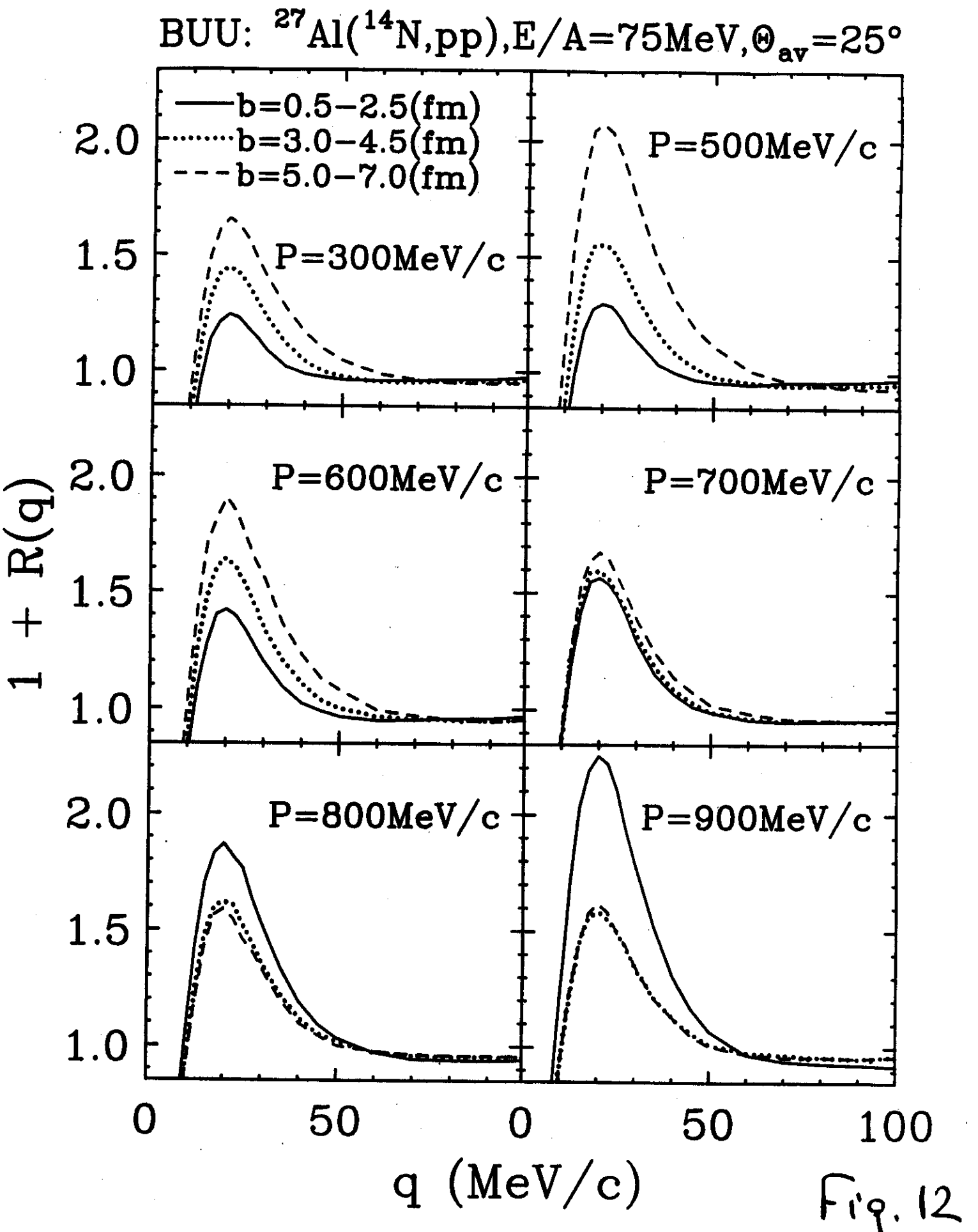
BUU: ^{27}Al(^{14}N,pp),E/A=75MeV,Θ_{av}=25°
b=0.5–2.5(fm)
b=3.0–4.5(fm)
b=5.0–7.0(fm)
P=300MeV/c
P=500MeV/c
P=600MeV/c
P=700MeV/c
P=800MeV/c
P=900MeV/c
1 + R(q)
q (MeV/c)
0
50
100
1.0
1.5
2.0

Fig. 12

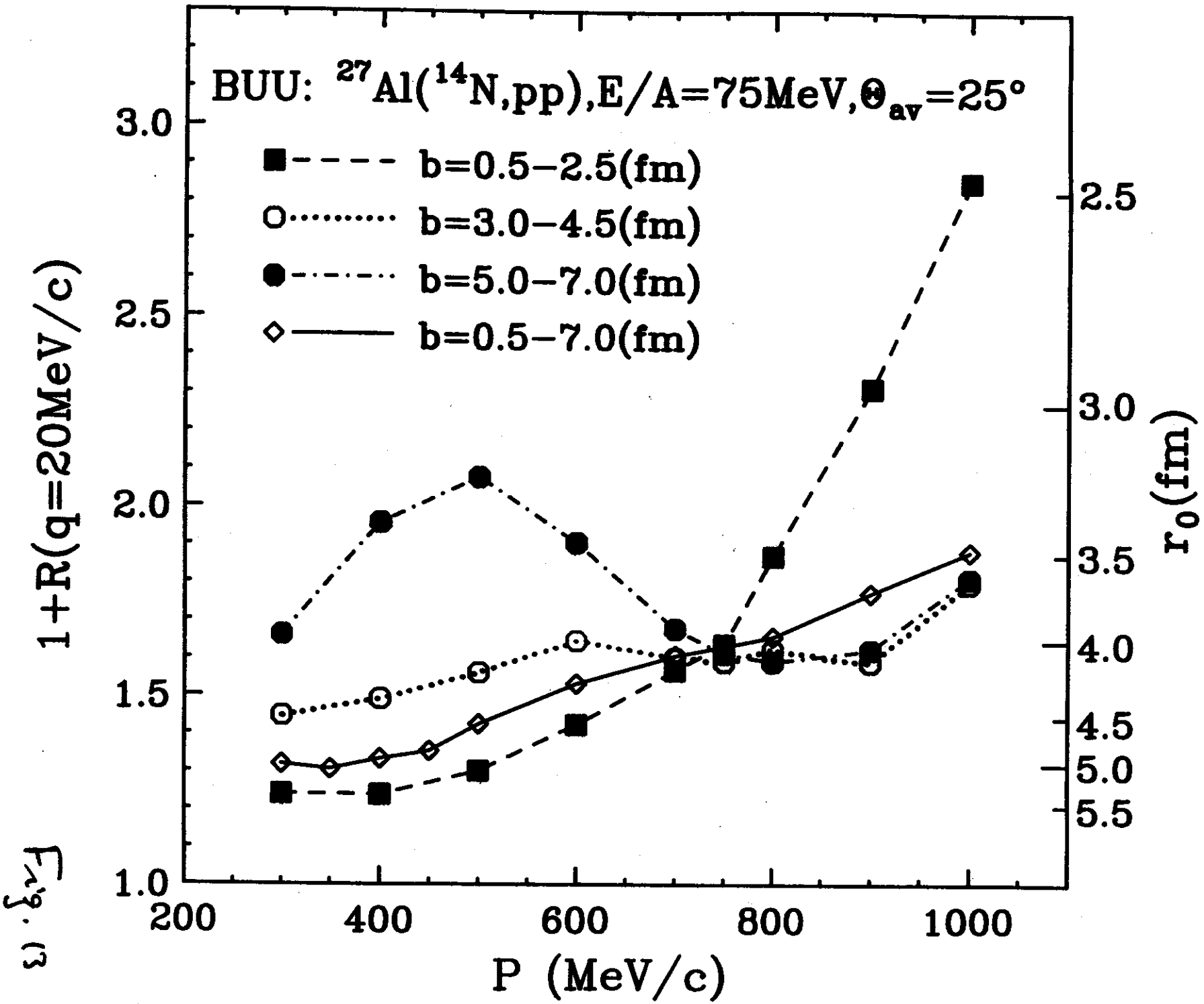
BUU: ^{27}Al(^{14}N,pp),E/A=75MeV,θ_{av}=25°
b=0.5–2.5(fm)
b=3.0–4.5(fm)
b=5.0–7.0(fm)
b=0.5–7.0(fm)
1+R(q=20MeV/c)
r_0(fm)
P (MeV/c)
3.0
2.5
2.0
1.5
1.0
2.5
3.0
3.5
4.0
4.5
5.0
5.5
200
400
600
800
1000

Fig. 3

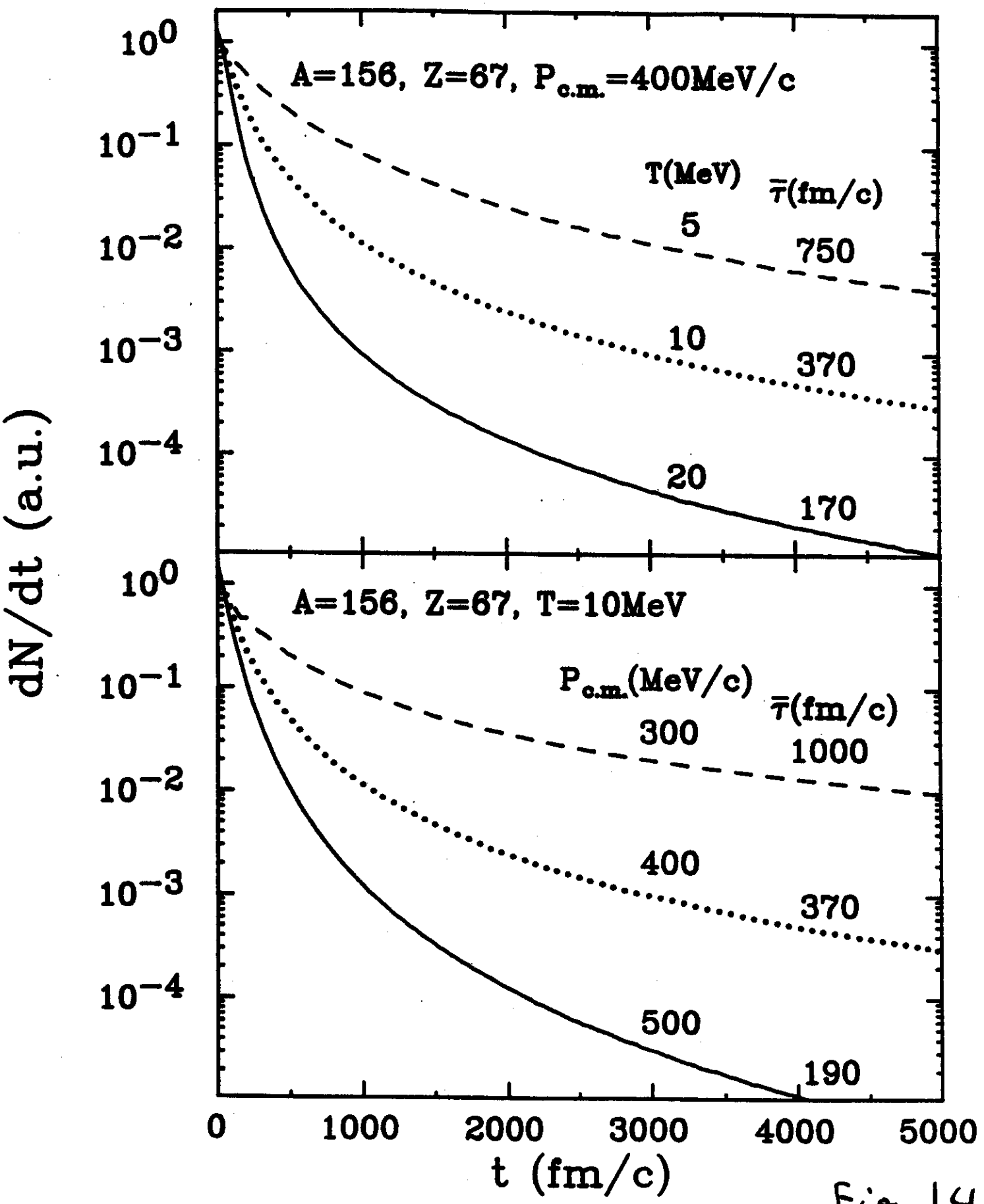
A=156, Z=67, P_c.m.=400MeV/c
T(MeV)
τ̄(fm/c)
5
750
10
370
20
170
A=156, Z=67, T=10MeV
P_c.m.(MeV/c)
τ̄(fm/c)
300
1000
400
370
500
190
dN/dt (a.u.)
t (fm/c)
10^0
10^-1
10^-2
10^-3
10^-4
0
1000
2000
3000
4000
5000

Fig. 14

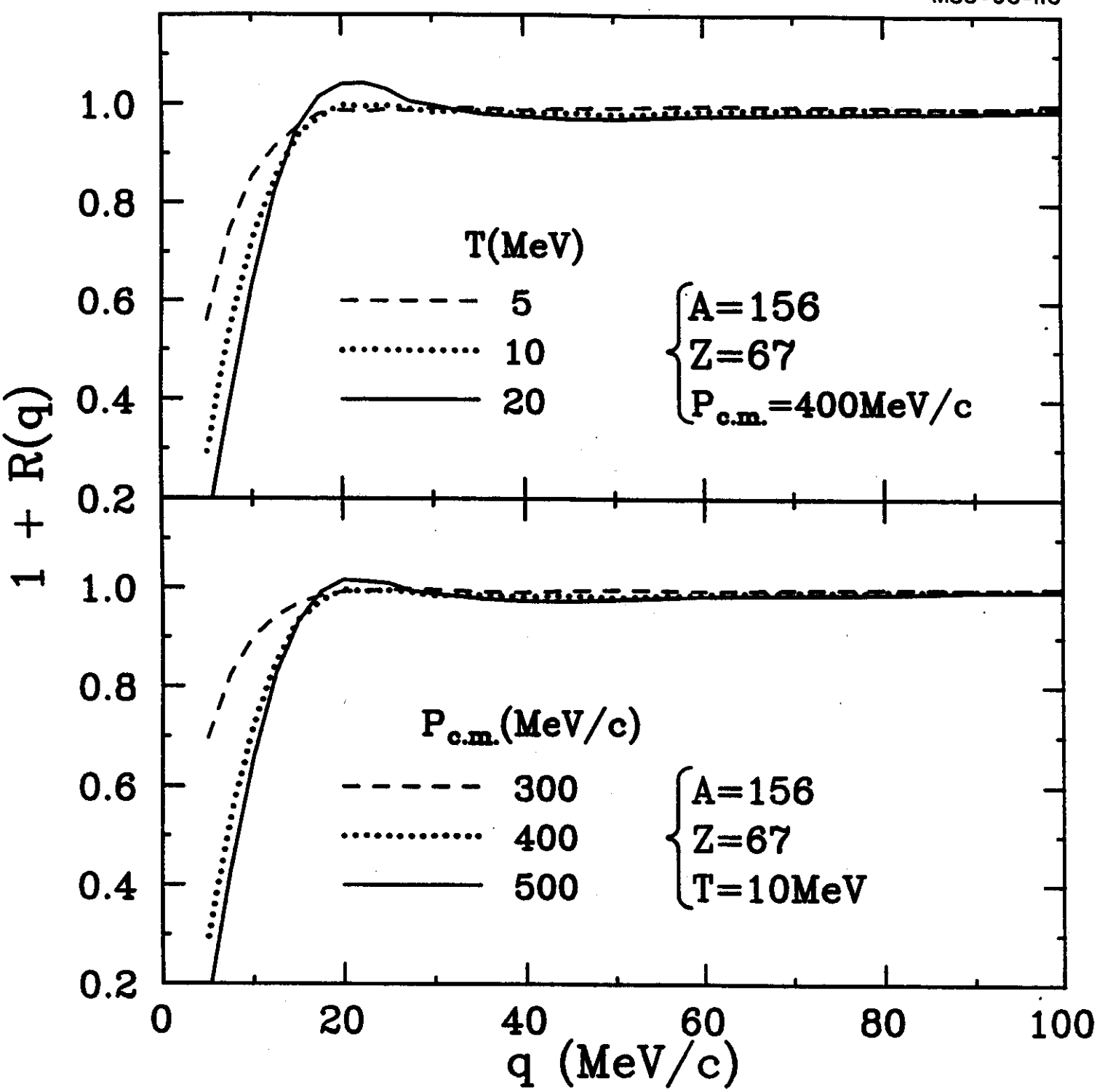
1 + R(q)
1.0
0.8
0.6
0.4
0.2
T(MeV)
5
10
20
A=156
Z=67
P c.m.=400MeV/c
P c.m.(MeV/c)
300
400
500
A=156
Z=67
T=10MeV
0
20
40
60
80
100
q (MeV/c)

Fig. 15

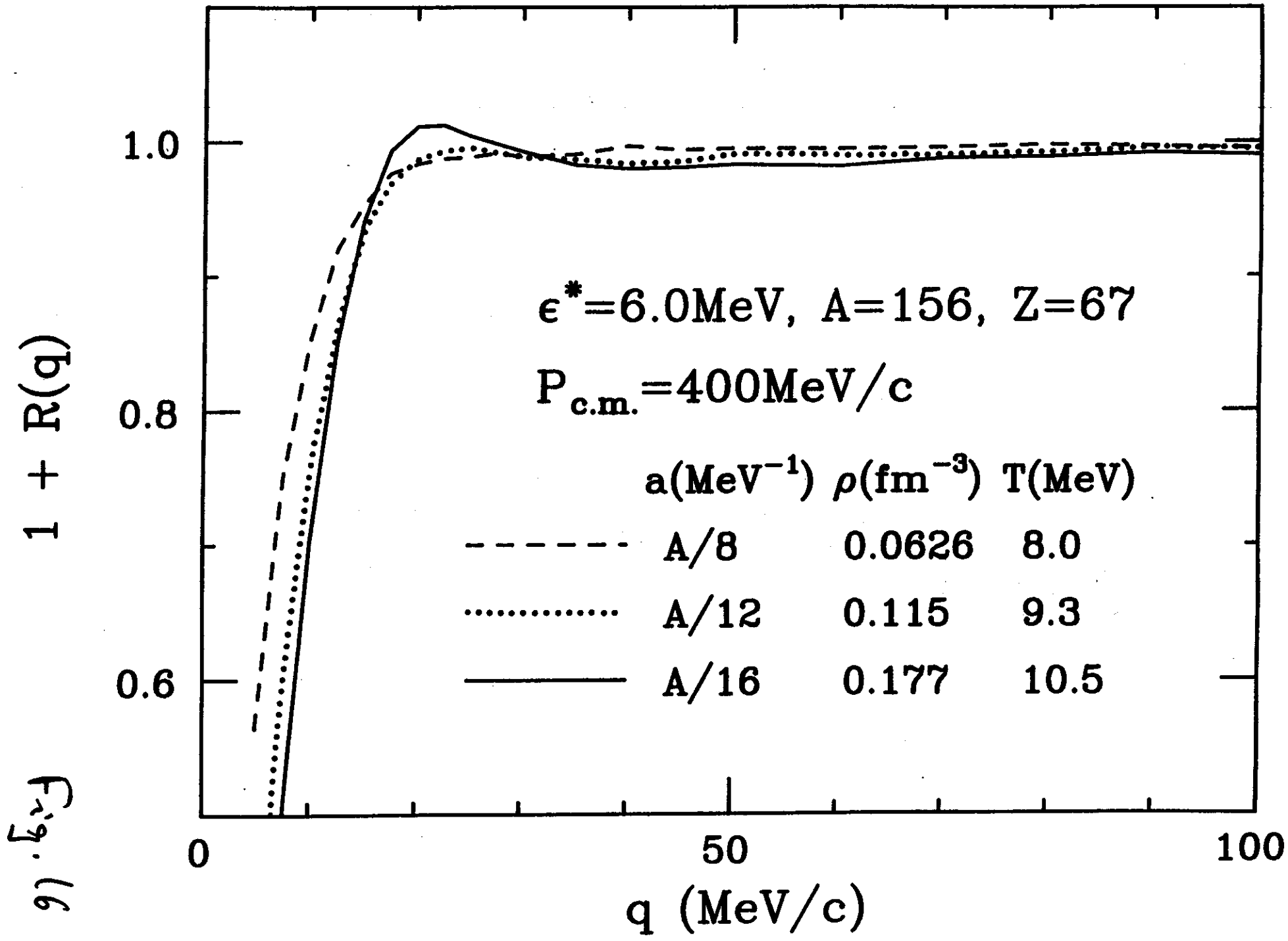
1.0
0.8
0.6
1 + R(q)
0
50
100
q (MeV/c)
ϵ^*=6.0MeV, A=156, Z=67
$P_{c.m.}$=400MeV/c
a(MeV^{-1}) ρ(fm^{-3}) T(MeV)
A/8 0.0626 8.0
A/12 0.115 9.3
A/16 0.177 10.5

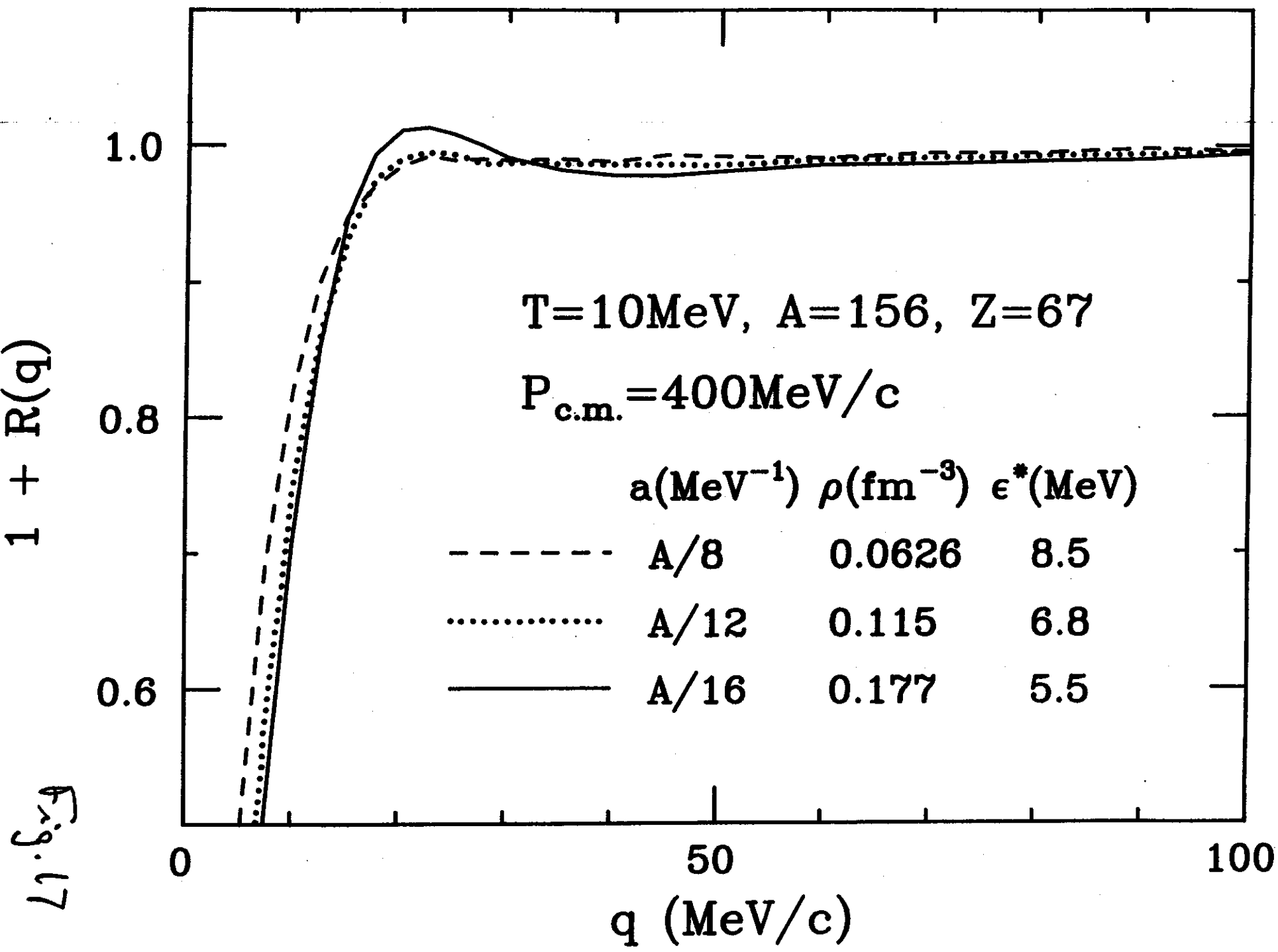
1.0
0.8
0.6
1 + R(q)
0
50
100
q (MeV/c)
T=10MeV, A=156, Z=67
P c.m.=400MeV/c
a(MeV⁻¹) ρ(fm⁻³) ε*(MeV)
A/8 0.0626 8.5
A/12 0.115 6.8
A/16 0.177 5.5

Fig. 17

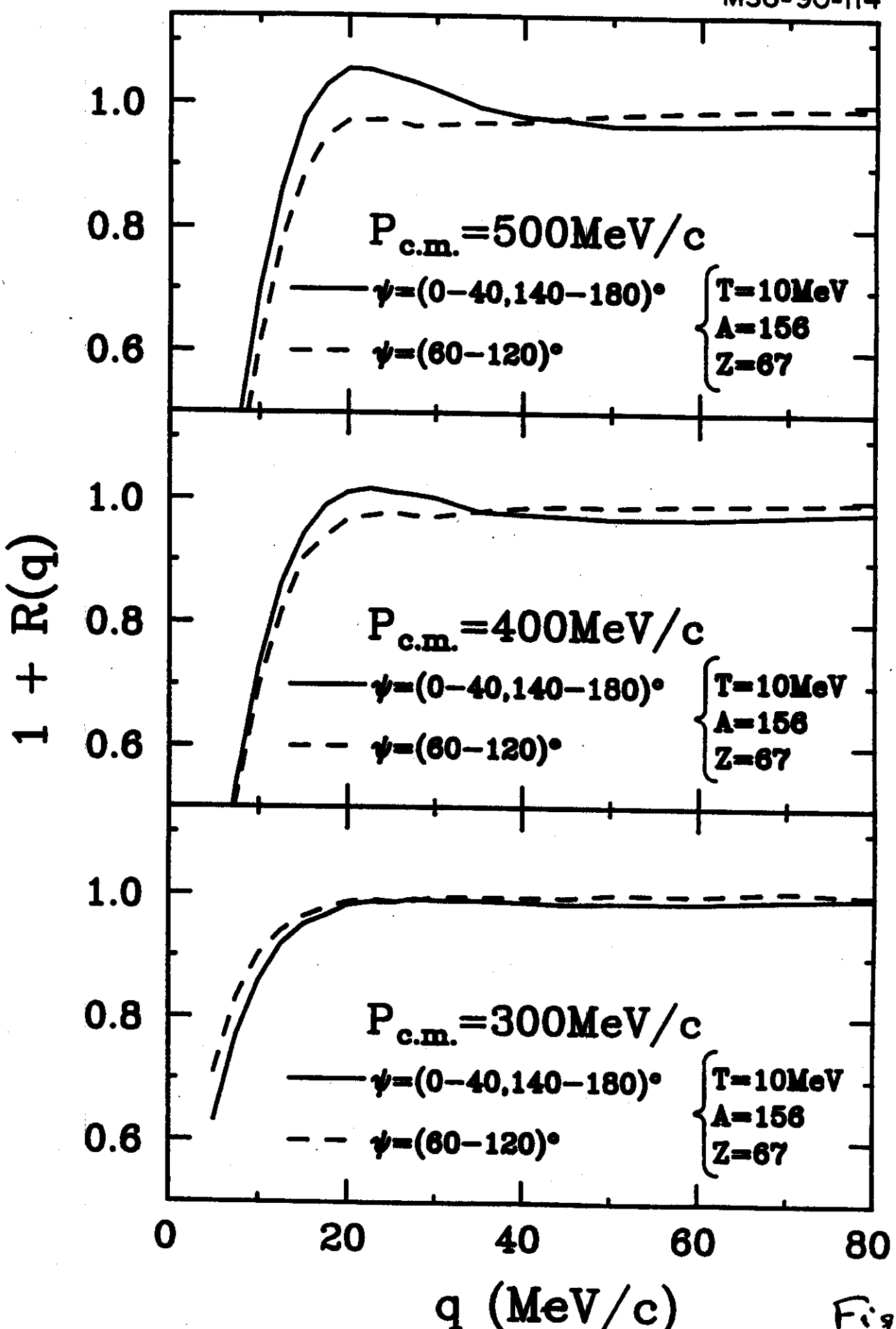
1 + R(q)
1.0
0.8
0.6
$P_{c.m.}$=500MeV/c
ψ=(0–40,140–180)°
ψ=(60–120)°
T=10MeV
A=156
Z=67
$P_{c.m.}$=400MeV/c
ψ=(0–40,140–180)°
ψ=(60–120)°
T=10MeV
A=156
Z=67
$P_{c.m.}$=300MeV/c
ψ=(0–40,140–180)°
ψ=(60–120)°
T=10MeV
A=156
Z=67
0
20
40
60
80
q (MeV/c)

Fig. 18